Preparation and Modification of Recoverable Particle Catalysts for Coal Liquefaction

Isao Mochida, Kinya Sakanishi, Hideki Taniguchi, Haru-umi Hasuo, and Osamu Okuma[+)]
Institute of Advanced Material Study, Kyushu University, Kasuga, Fukuoka 816, Japan
[+)]Polymer & Chemical Technology Lab., Kobe Steel, Ltd., Kobe, Hyogo 651-22, Japan

INTRODUCTION

Highly active catalyst of higher activity is still a key to design the more efficient coal liquefaction process, which will increase the oil yield, minimize its cost, and environmental impact due to catalyst disposal.

The authors assumed that the recovery and recycle of the catalyst from the residue are an approach to improve the economy of coal liquefaction and to reduce the solid waste.[1,2] The organic residue has been recycled with the catalyst and minerals to the primary liquefaction stage as the bottom recycle. Its favorable results have been reported, although the accumulation of the inorganic solid requires a fixed rate of purging the catalyst as well as minerals.

The authors have examined Fe_3Al, strong ferromagnetic particles, as one of the potentially recoverable catalysts[1,2], in order to prepare an active catalyst with the recovery function through magnetic separation.

Ketjen Black(KB) particles have hollow spheric structure which carries their extremely high surface area and for high dispersion of catalytic species and low specific gravity for catalyst recovery through the gravimetric separation. The activity of carbon particles and their supporting NiMo catalysts have been reported,[3-5] to exhibit the high activity for the hydrogen transferring cracking, hydrodesulfurization and hydrocracking. KB-supported NiMo catalyst is expected to be one of the most prmising catalysts to exhibit a large activity for hydrogenation and liquefaction at its least catalyst amount. To achieve the successful reuse of recovered catalyst, the deactivation, contamination, and adhesion of the catalyst should be avoided by designing the liquefaction and distillation schemes. The pretreatment and hydrogen transferring liquefaction prior to the catalytic steps are responsible to define the forms of minerals and to reduce the coke precursors[6-8]. Separation of the catalyst should assure its dispersed state.

In the present study, two types of recoverable catalysts were examined in terms of catalytic activities for the liquefactions of Wyoming coal (USA) and Tanitohalm coal (Indonesia). Optimization of reaction conditions and design of recovery procedures were studied in order to practice recovery and recycle of the catalysts in the liquefaction of both coals as well as to increase the oil yield with the least yield of organic residue.

EXPERIMENTAL

Some properties of Ketjen Black(KB) EC and JD, and Fe_3Al examined in the present study are summarized in Table 1. Ni, Mo-supported KB catalysts (NiMo/KB) were prepared by impregnation method from $Ni(NO_3)_2$ or $Ni(OAc)_2$ and $(NH_4)_6Mo_7O_{24}$ or Mo dioxyacetylacetonate (MoO_2-AA) in their water or methanol solutions, respectively. The catalyst precursors were dried at 120℃ for 12 h in vacuo and presulfided in 5% H_2S/H_2 flow at 360℃ for 2 or 3 h prior to the reactions. KB was pretreated in conc. nitric acid at 80℃ for 1 h followed by filtration, repeated washing with water, and drying at 120℃ in vacuo. The nitric acid-treated KB JD was abbreviated as KB JD-O.

Synthetic pyrite powder and KF842 ($NiMo/Al_2O_3$, pellet or its powder (<60 mesh)) provided by NEDO and Nippon Ketjen Co., respectively were also used as the reference catalysts for the comparison. These catalysts and Fe_3Al particles were also presulfided under the same conditions as KB-based catalysts.

The elemental analyses of Wyoming and Tanitohalm coals are summarized in Table 2. Tetralin (TL) of commercial guaranteed grade was used as a liquefaction (hydrogen donating) solvent. The liquefaction was carried out in an autoclave of 50 ml capacity (11 or 20℃/min) at the prescribed temperatures(380 - 460℃). The coal (3.0 g) , the solvent (4.5 g) and catalyst (0.09 - 0.10 g) were charged into the autoclave, which was then pressurized with hydrogen to 6~ 9.3 MPa at room temperature after replacing the air with nitrogen gas. After the reaction, the product remaining in the autoclave was recovered with THF, and extracted in sequence with hexane, acetone and THF after evaporating THF. The hexane soluble (HS), hexane insoluble-acetone soluble (HI-AS), acetone insoluble-THF soluble (AcI-THFS), and THF insoluble (THFI) substances were defined as oil(O), asphaltene(A), preasphaltene(PA), and residue(R), respectively. The gas yield was calculated by the difference between weights of the initial coal and recovered product.

RESULTS AND DISCUSSIONS

Liquefaction of Wyoming Coal with KB-supported NiMo Catalyst

Figure 1 illustrates the effects of reaction temperatures on the liquefaction of Wyoming coal with KB-ED-supported NiMo catalyst under initial H_2 pressure of 6.6 MPa at 380 - 460℃. The oil yield increased with reaction temperature in the ragne of 380 - 440℃, reaching the maximum oil yield of 40 % at 440℃, and then decreased at 460℃ with a singnificant increase of gas yield.

Figure 2 shows the comparative activity of the KB JD-O-supported NiMo catalyst prepared by the successive impregnation method with the commercial $NiMo/Al_2O_3$ catalyst and synthesized pyrite for the liquefaction of Wyoming coal at 440℃ for 20 min. The KB-supported NiMo catalyst gave the higher oil and asphaltene yields with less yields of preasphaltene and residue. The commercial NiMo and pyrite catalysts provided the lower oil plus asphaltene yields with higher gas and preasphaltene yields and higher asphaltene yield, respectively.

Liquefaction of Tanitohalm Coal with Recoverable Catalysts

Figures 3 and 4 compare liquefaction results of Tanitohalm coal without and with sulfided Fe_3Al(Fe_3Al-S), NiMo/KB-JD, and synthetic pyrite at 450℃ for 60 min under the initial H_2 pressures of 6.0 and 9.3 MPa, respectively. The sulfided NiMo/KB-JD catalyst exhibited the highest activity for the much higher oil yield over 60 % under the higher hydrogen pressure. It is noted that the much lower yields of preasphaltene and residue were obtained in the liquefaction of Tanitohalm coal compared to those of Wyoming coal. The pyrite showed the similar activity as NiMo/KB-JD under the lower hydrogen pressure, although it failed in increasing the oil yield under the higher hydrogen pressure. Sulfided Fe_3Al particles do not essentially show any activity even after the grinding to smaller particle size under the present reaction conditions.

Figures 5 and 6 illustrate the liquefaction of Tanitohalm coal with NiMo/KB-JD catalyst at 380 - 450℃ under the initial H_2 pressures of 6.0 and 9.3 MPa, respectively. The oil yield increased very much with reaction temperatures under the higher hydrogen pressure, reaching the maximum yield of 62% with least yields of preasphaltene and residue. In contrast, the oil yield appeared to be saturated around 45% in the temperature range of 420 - 450 ℃, while the yields of asphaltene, preasphaltene and residue decreased and the gas yield increased sharply.

Recovery and repeated use of recoverable catalysts

The magnetically recoverable Fe_3Al particles were found to be more easily recovered from the whole liquefaction product than from the THFI residue, because the mineral matters and organic residue in THFI were strongly adhered together to include the catalyst in the grains, making it difficult to recover the catalyst separately.

Ketjen black supporting catalysts were found to be recovered from the whole product by gravimetric floatation technique using methanol, hexane and water in this order, although the weight of recovered catalyst was gained to some extent probably due to the inclusion of organic materials on the catalyst.

The KB-supported catalyst and Fe_3Al were found recoverable after the liquefaction, although some carbon adhesion took place. The KB-supported catalyst exhibited an excellent activity for the coal liquefaction. Addition of acidic properties may provide higher activity for the asphaltene conversion. Fe_3Al is found to have very small activity. Its application as the catalyst support can be examined.

The multi-stage approach consisting of coal pretreatment, solvent-mediated dissolution, and catalytic hydrocracking steps should be furhter developed to suppress the catalyst deactivation.

References

1) Mochida,I., Sakanishi,K., Kishino,M., Honda,K., Umezawa,T., Yoon,S.H., ACS Div.Fuel Chem., 1993, 38(1), 93.

2) Mochida,I., Sakanishi,K., Sakata,R., Honda,K., Umezawa,T., Energy & Fuels, 1994, 8, 25.

3) Derbyshire, F.J., DeBeer, V.H.J., Abotsi, G.M.K., Scaroni, A.W., Solar, J.M., Skrovanok,D.J., Appl.Catal., 1986, 27, 117.

4) Farcasiu,M., Smith,C., Energy & Fuels, 1991, 5, 83.

5) Duchet,J.C., van Oers,E.M., de Beer,V.H.J., Prins,R., J.Catal., 1983, 80, 386-402

6) Mochida,I., Yufu,A., Sakanishi,K., Korai,Y., Fuel, 1988, 67, 114.

7) Mochida,I., Kishino,M., Korai,Y., Sakanishi,K., J.Fuel Soc. Jpn., 1986, 65, 828.

8) Mochida,I., Sakata,R., Sakanishi,K., Fuel 1989, 68, 306.

Table 1 Some properties of KB carbon blacks and Fe_3Al particles

Samples	Particle size (μ m)	Surface area (m^2/g)	Specific gravity (-, H_2O=1)
Fe_3Al	7.2(<500 mesh)	0.5	6.5 - 7.9
KB-EC	30×10^{-3}	800	0.145
KB-JD	30×10^{-3}	1270	0.115

Table 2 Elemental analyses of coals

	wt%, daf basis				H/C	Ash
	C	H	N	(O+S)	(-)	(wt%)
Wyoming	68.9	5.4	1.0	24.7	0.94	3.7
Tanitohalm	75.9	5.6	1.5	17.1	0.87	4.8

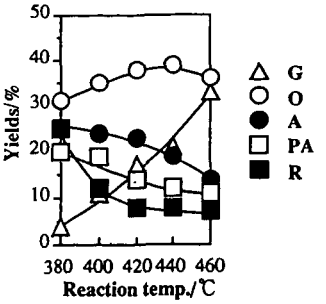

Fig.1 Effect of reaction temperature on the liquefaction of Wyoming coal.

solvent(Tetralin)/coal=1.5
reaction time : 40min
H_2 initial pressure : 6.6MPa
catalyst : Ni-Mo/KB EC(Ni2wt%,Mo10wt%/simultanious impregnation from $Ni(NO_3)_2$ and $(NH_4)_6Mo_7O_{24}$)
3%addition based on coal presulfided at 360℃ for 3h

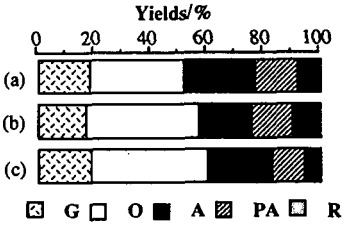

Fig.2 Effect of catalysts species on the liquefaction of Wyoming coal at 440℃

(a) Synthsized FeS_2
(b) Commercial Ni-Mo/Al_2O_3
(Ni:3wt%,Mo:15wt%)
(c)Ni-Mo/KB JD-O(MoO_2-AA, $Ni(OAc)_2$ successive impregnation)
reaction temperature : 440℃
reaction time : 20min
(Other conditions are same as Fig.1)

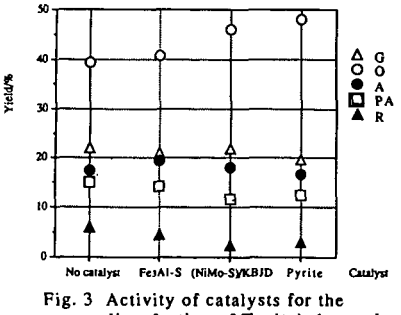

Fig. 3 Activity of catalysts for the liquefaction of Tanitohalm coal under lower H_2 pressure
solvent(Tetralin)/coal(Tanitohalm)=1.5
Reaction time 60min, Reaction temp. 450℃
Heatig rate 20℃/min, H_2 initial press. 6.0MPa

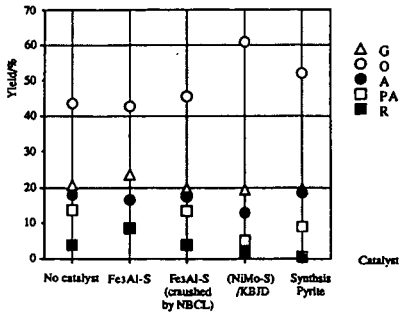

Fig. 4 Activity of catalysts for the liquefaction of Tanitohalm coal under higher H_2 pressure

solvent(Tetralin)/coal(Tanitohalm)=1.5
Reaction time 60min, Reaction temp. 450℃
Heatig rate 20℃/min, H2 initial press. 9.3MPa

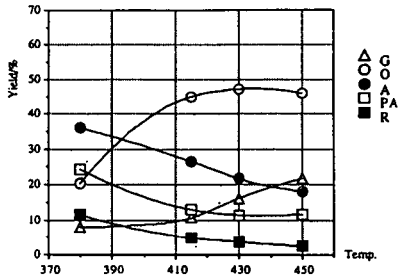

Fig. 5 Effect of reaction temperature on the liquefaction of Tanitohalm coal under lower H_2 pressure

solvent(Tetralin)/coal(Tanitohalm)=1.5
Reaction time 60min, Heatig rate 20℃/min
H2 initial press. 6.0MPa
catalyst:NiMo/KB JD(Ni:2wt%,Mo10wt%)
3wt% addition based on coal presulfided at 360℃ for 2h

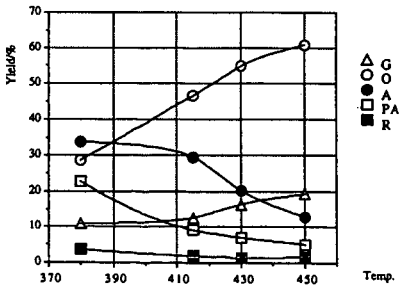

Fig. 6 Effect of reaction temperatures on the liquefaction of Tanitohalm coal under higher H_2 pressure

solvent/coal=1.5
Reaction time 60min, Heatig rate 20℃/min
H2 initial press. 9.3MPa
catalyst:NiMo/KB JD(Ni:2wt%,Mo10wt%)
3wt% addition based on coal presulfided at 360℃ for 2h

COMPARISON OF THE ACTIVITIES OF FINE-PARTICLE SIZE CATALYSTS*

Frances V. Stohl, Kathleen V. Diegert, David C. Goodnow
Process Research Department 6212
Sandia National Laboratories
P.O. Box 5800
Albuquerque, NM 87185-0709

ABSTRACT

The objectives of Sandia's fine-particle size catalyst testing project are to evaluate and compare the activities of the fine-particle size catalysts being developed in DOE/PETC's Advanced Research Coal Liquefaction Program by using standard coal liquefaction test procedures. The standard procedures use Blind Canyon coal, phenanthrene as the reaction solvent, and a factorial experimental design with temperatures from 350°C to 400°C, reaction times from 20 to 60 minutes, and catalyst loadings up to 1 wt%. Catalytic activity is measured in terms of tetrahydrofuran conversion, heptane conversion, the amount of 9,10-dihydrophenanthrene in the product, and the gas yield. Several catalysts have been evaluated including a commercially available pyrite, a sulfated iron oxide from the University of Pittsburgh, and several preparations of 6-line ferrihydrites from Pacific Northwest Laboratories. Results have demonstrated that significant differences in activity can be detected among these catalysts.

INTRODUCTION

There are several potential advantages of using cheap, unsupported, fine-particle size (<40 nm) catalysts in direct coal liquefaction. These include improved coal/catalyst contact due to good dispersion[1] of the catalyst, and the potential for using low quantities of catalyst (≤0.5% based on the weight of coal) because of their very high surface areas. These catalysts could be combined with the coal as either active catalysts or catalyst precursors that would be activated in situ. Research efforts that have been performed to develop fine-particle size, unsupported catalysts for direct coal liquefaction[2] indicate that the use of these catalysts could result in significant process improvements, such as enhanced yields of desired products, less usage of supported catalyst, and possibly lower reaction severities. These improvements would result in decreased costs for coal liquefaction products.

The Advanced Research (AR) Coal Liquefaction Program, which is managed by the United States Department of Energy's Pittsburgh Energy Technology Center (PETC), is funding numerous research efforts aimed at developing these types of catalysts for direct liquefaction. Although most catalyst developers have the capability of testing the performances of the catalysts they develop, it is difficult if not impossible to compare results among researchers because of the different testing procedures used. Therefore, to guide the research and development efforts for these fine-particle size, unsupported catalysts, it is necessary to evaluate each catalyst's performance under standard test conditions so that the effects of catalyst formulations from different laboratories can be compared.

The objectives of this project are to develop standard coal liquefaction test procedures, to perform the testing of the novel fine-particle size liquefaction catalysts being developed in the PETC AR Coal Liquefaction program, and to evaluate reaction mechanisms. Previously reported work[3,4] described the reaction procedures, product workups, and the factorial experimental design to be used in this project as well as results obtained by testing a commercially available pyrite and the University of Pittsburgh's sulfated iron oxide catalyst. This paper will describe the recent results obtained from evaluating a Pacific Northwest Laboratories' (PNL) catalyst.

EXPERIMENTAL SECTION

Materials. The coal being used in this project is the DECS-17 Blind Canyon Coal obtained from The Penn State Coal Sample Bank. It is a high volatile A bituminous coal with 0.36% iron, 0.02% pyritic sulfur, and 7.34% mineral matter (on a dry basis). The particle size is -60 mesh. Phenanthrene is used as the reaction solvent. Elemental sulfur was added to the reactors to sulfide the catalyst precursors.

Microautoclave Reactors. The testing is performed using batch microautoclaves made of type 316 stainless steel components. The total volume of a reactor is 43 cm^3 with a liquid capacity of 8 cm^3. The reactors are loaded with 1.67g coal and 3.34g reaction solvent. If the reaction is catalytic, the catalyst loading will be either 0.5 wt% or 1.0 wt% on an as-received coal basis. The amount of sulfur addition is specified by the catalyst developer. The reactors are charged to 800 psig H_2 (cold charge) and heated to reaction temperatures in fluidized-sand baths. Temperatures, pressures and times are recorded with a digital data acquisition system every 30 seconds during the course of the reactions. Following the heating period, the reactors are rapidly cooled to ambient temperature in a water bath and a gas sample is collected. The reaction data is analyzed to determine the actual reaction time and the averages and standard deviations for reaction temperature and pressure. Heat-up times and cooling times are also determined.

Product Workup Procedures. The reaction products are rinsed out of the reactors with tetrahydrofuran (THF). THF and heptane solvent solubilities are measured using a Millipore 142 mm diameter pressure filtration device with air pressurization and Duropore (0.45 micron) filter paper. The filter cakes are rinsed twice with THF or heptane as appropriate. After the filtrations are complete, the filter papers are dried under vacuum at 70°C, cooled to room temperature and weighed to determine the insoluble portions. The THF soluble material is quantitatively sampled for gas chromatographic (GC) analysis, which is used to determine the reaction solvent recovery and composition. The THF is removed from the solubles by rotary evaporation prior to determining the heptane conversion. The quantity of gases (CO, CO_2, CH_4, C_2H_6) produced in a reaction is calculated using the postreaction vessel temperature and pressure with the ideal gas law and the mole percents in the gas sample as determined using a Carle GC and standard gas mixtures.

Factorial Experimental Design and Analysis. The factorial experimental design (Figure 1) evaluates the effects of three variables at two levels: temperature (350 and 400°C), time (20 and 60 minutes), and catalyst loading (0 and 1 wt% based on as-received coal). With this full factorial experimental design, the experimental results are evaluated for all combinations of levels of the three variables so that 2^3 evaluations are required. Additional reactions are also performed at the center point of this cubic design. An Analysis of Variance (ANOVA) is performed to estimate the effects of the experimental variables and to statistically test their significance. Replication of the experiments is used to estimate measurement error and to reduce its effect on the estimated effects of the variables. Models are constructed using the estimates of the effects of the variables to calculate the expected experimental results for specified sets of reaction conditions[5]. The controlled factors used in the ANOVA are the measured average reaction temperature, measured reaction time, and the actual weight of catalyst used.

Catalyst. J. Linehan (PNL) supplied Sandia with the -325 mesh fraction of a 6-line ferrihydrite catalyst precursor for evaluation using the full factorial experimental design. No pretreatment was required. Linehan recommended testing this material with a 1:1 sulfur to catalyst precursor ratio on a weight basis. All reactions including thermal reactions had the same amount of added sulfur, so the impact of sulfur could be determined.

RESULTS and DISCUSSION

Experimental Results of Testing PNL's 6-Line Ferrihydrite Catalyst
The testing of PNL's 6-line ferrihydrite catalyst precursor plus sulfur was performed by two operators: operator 1 (a previous operator) and operator 2 (the current operator). The measured experimental results obtained by operator 2 using the full factorial experimental design are given in Table 1. The reproducibility of the measured THF conversions is good for most of the data. However, results at 350°C for 60 minutes show high variability These reaction products were significantly more difficult to filter than those from other conditions; the reason for this is unknown. Negative values for heptane conversion occur because the values are very close to zero, and the variability is high.

Modeling of Experimental Results
Results of the statistical analyses of the data in Table 1 are given in Tables 2 and 3. These tables show calculated estimates of the effects of the variables and the interactions among variables over the region bounded by the cubic design, calculated estimates of the mean values of the reaction results at the nine sets of reaction conditions, standard errors of the estimates, the means of the measured values in Table 1, and R^2 values for the fit of the model to the data. The constant represents the estimate of the reaction results when all variables are at their low levels: temperature=350°C, time=20 minutes, and catalyst loading=0%. The variables with statistically significant effects are listed under the constant; the larger the estimated value, the greater the effect. The estimate of experimental error, which is presented as a standard deviation, accounts for all variability in the data not accounted for by the fixed and random effects of the model. Included in this estimate are variabilities due to measurement, process and material inconsistencies, and modeling inadequacies. The estimates of reaction results at the nine sets of reaction conditions are calculated from the model and can be compared to the means of the measured values. The standard errors of the estimated results at cube corners are derived from the experimental error, which pertains to a single measurement.

The results of the modeling show that temperature has the largest effect on both the THF (33.6%) and heptane (17.5%) conversions. The catalyst has the second largest effect on THF conversion (16.6%) but no significant effect on heptane conversion. The lack of catalytic effect on heptane conversion was also observed when pyrite and the University of Pittsburgh's catalyst were evaluated.[3,4] The other significant parameters for THF conversion are time (11.5%) and the temperature-catalyst interaction (9.3%). For heptane conversion the other significant parameters are the time-temperature interaction (7.5%) and time (2.8%). The significant effects for gas yield are temperature (0.91%), the time-temperature interaction (0.43%) and time (0.23%). The 9,10-dihydrophenanthrene (DHP), which was formed by hydrogenation of phenanthrene, in the reaction product has the most complicated model with six parameters having significant effects: temperature-catalyst interaction (2.83%), time-catalyst interaction (2.39%), temperature (1.03%), catalyst (0.85%), time-temperature interaction (0.52%), and time (0.40%). The R-square values for the fit of the models were 0.94 for THF conversion and 0.96 for the other three models.

Procedure for Estimating Experimental Results from the Linear Model. To use one of the linear models in Tables 2 or 3 to determine an estimate for an experimental result within the cube, first calculate proportional levels for each variable that has a significant effect. For example, to calculate THF conversion for a reaction at 375°C for 40 minutes with 0.5% catalyst:

p_{TIME}=(40 min-20 min)/(60 min-20 min)=0.5
p_{TEMP}=(375°C-350°C)/(400°C-350°C)=0.5
p_{CAT} =(0.5 wt%-0 wt%)/(1.0 wt%-0 wt%)=0.5

These calculated p's are used in the following equation (see Table 2):

$$K + p_{TIME}\cdot a + p_{TEMP}\cdot b + p_{CAT}\cdot c + p_{TEMP}\cdot p_{CAT}\cdot d$$

where K is the estimated constant (18.5%), a is the estimated time effect (11.5%), b is the estimated temperature effect (33.6%), c is the estimated catalytic effect (16.6%) and d is the estimated temperature-catalyst interaction (9.3%). The calculated THF conversion is 51.7, which agrees within round off errors with the value in Table 2. For calculating a result for any point within the region

bounded by the cube, the p values will range from 0 to 1. Extrapolation beyond the limits of the cube is usually not recommended.

Evaluation of Operator Effects

To compare results from the University of Pittsburgh's catalyst and PNL's catalyst, it is necessary to evaluate operator effects. The testing of PNL's catalyst using the full experimental design (Table 1) was performed by operator 2, whereas operator 1 performed the evaluation of the University of Pittsburgh's catalyst as well as a limited number of reactions on PNL's catalyst. The experiments performed by each operator on PNL's catalyst are shown in Table 4. A statistical analysis of the THF conversion results for operator 2 (Table 1) showed that a model (Table 2) with significant effects for temperature, catalyst, time and the temperature-catalyst interaction fit the data well (R^2=0.94). To compare the results from the two operators, operator 2's data for reactions at 350°C for 20 minutes were not used because operator 1 had not performed these reactions. Results of the comparison are shown in Table 5. The values in Table 5 for the model of THF conversion obtained by operator 2 are slightly different from those in Table 2 because Table 2's results included reactions performed at 350°C for 20 minutes.

Comparison of the constants for the two operators shows that there are significant differences in THF conversions at 350°C for 20 minutes without catalyst. Using these two models to calculate THF conversion at 375°C for 40 minutes with 0.5% catalyst (the center point of the experimental design) gave 56.7% for operator 1 and 49.9% for operator 2. Calculating results at 400°C for 60 minutes with 1wt% catalyst gave a THF conversion of 88.4% for operator 1 and a similar value of 87.5% for operator 2. Comparison of these three sets of calculated results shows that the biggest differences between the two operators were at the lowest severity conditions. Because of these differences, only the high severity results are compared in Table 6. The estimates of error variability (within their respective data sets) were comparable for the two operators. Similar conclusions were obtained for comparison of heptane conversion results between the two operators. Operator 1 had higher conversions than operator 2, particularly at low temperature. Unfortunately, a model for heptane conversion could not be fit for operator 1 results, because the time-temperature interaction is important for heptane conversion, and operator 1 did not perform tests at 350°C for 20 minutes.

Comparison of Catalysts

A comparison of results (Table 6) from PNL's catalyst with results from the University of Pittsburgh's catalyst and pyrite at the higher severity conditions indicates that PNL's catalyst is the most active. THF results show that PNL's catalyst increases conversion by 25.8% over it's thermal baseline with 1% sulfur addition. The University of Pittsburgh's catalyst and pyrite increase conversion above their respective baseline values by 19.3% and 18.5% respectively. Comparison of the three baseline results shows that sulfur addition has an effect on THF conversion. Therefore, the best comparison among these three catalysts is obtained by using the thermal baseline without sulfur addition (54.9%). Using this baseline gives 34.5% total conversion for PNL's catalyst, 27.4% conversion for the University of Pittsburgh's catalyst and 18.5% for pyrite.

The model for the amount of DHP (Table 3) in the recovered reaction solvent from experiments performed with PNL's catalyst involved the three main effects (time, temperature, catalyst) as well as the three two-way interactions (time-temperature, time-catalyst, temperature-catalyst). This model is somewhat simpler than those obtained for pyrite and the University of Pittsburgh's catalyst, because it doesn't have the three-way interaction. The amount of DHP present in the product from the 400°C reaction for 60 minutes with PNL's catalyst was 8.41%. The University of Pittsburgh's catalyst yielded 5.35% DHP and pyrite yielded 3.88%. These results indicate that PNL's catalyst has the highest hydrogenation activity.

CONCLUSIONS

Results of the evaluation of PNL's 6-line ferrihydrite with 1 wt% sulfur addition have shown that it is more active than either the University of Pittsburgh's sulfated iron oxide with 2 wt% sulfur addition or pyrite. At 400°C for 60 minutes, THF conversion obtained with PNL's catalyst was 89.4% versus 82.3% with the University of Pittsburgh's catalyst, and 73.4% with pyrite. Analyses of DHP in the reaction products show that PNL's catalyst has the highest hydrogenation activity. PNL's catalyst gave 8.41% DHP, versus 5.35% for the University of Pittsburgh's catalyst, and 3.88% for pyrite. There were no catalytic effects for either heptane conversion or gas yield. Future work will involve testing additional catalysts being developed in DOE/PETC's program and evaluating better analytical methods for determining product quality.

ACKNOWLEDGEMENT: This work was supported by the U.S. Department of Energy at Sandia National Laboratories under contract DE-AC04-94-AL85000.

REFERENCES

1. Huffman, G. P.; Ganguly, B.; Zhao, J.; Rao, K. R. P. M.; Shah, N.; Feng, Z.; Huggins, F. E.; Taghiei, M. M.; Lu, F.; Wender, I.; Pradhan, V. R.; Tierney, J. W.; Seehra, M. S.; Ibrahim, M. M.; Shabtai, J.; Eyring, E. M.; Energy Fuels 1993, 7, 285-296.
2. Pradhan, V. R.; Tierney, J. W.; Wender, I.; Energy & Fuels 1991, 5, 497-507.
3. Stohl, F. V.; Diegert, K. V.; Energy & Fuels 1994, 8, 117-123.
4. Stohl, F. V.; Diegert, K. V.; Gugliotta, T. P.; Proc. Coal Liquefaction and Gas Conversion Contractors' Review Conf., September 27-29, 1993, Pittsburgh, PA. p. 123-135.
5. John, P. W. M.; Statistical Design and Analyses of Experiments; MacMillan Co., New York, 1971.

Figure 1. Factorial experimental design (temperature = °C, time = minutes, catalyst loading = wt% of as-received coal).

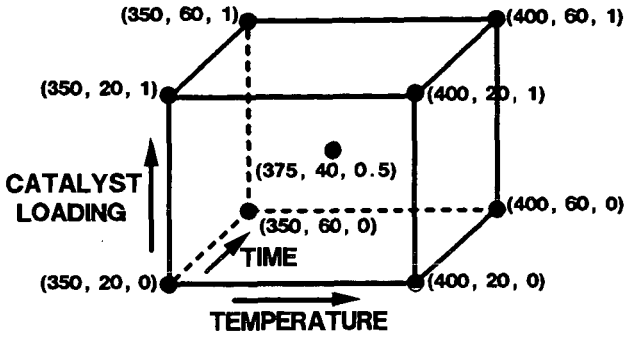

Table 1. Measured experimental results from operator 2.

TEMP. (°C)	TIME (min)	CAT. (mg)	THF Conv. (%)	Heptane Conv. (%)	Gas (%dmmf)	DHP (%)*
350.9	20.5	0	21.86	-2.63	0.34	0.33
349.4	20.5	0	17.28	-4.92	0.30	NA**
350.4	20.5	0	21.14	-1.56	0.25	NA
350.2	60.5	0	26.39	2.47	0.60	0.63
350.2	60.7	0	31.49	1.69	0.52	0.72
350.5	60.5	0	23.31	-2.15	0.44	0.60
349.9	59.0	0	26.98	1.43	NA	0.54
400.0	20.5	0	50.06	14.05	1.23	1.09
399.8	20.5	0	47.33	13.00	1.16	1.05
400.1	60.5	0	63.86	23.40	1.98	2.27
399.7	60.5	0	61.69	NA	1.82	2.36
375.1	40.5	8.4	63.52	7.90	0.83	3.97
374.8	40.5	8.6	56.89	8.59	0.78	4.00
374.8	40.5	8.1	62.12	5.19	0.76	3.78
375.1	41.0	8.3	57.11	8.02	0.75	2.96
375.4	40.5	8.4	54.24	8.48	0.78	3.67
350.5	20.5	16.6	35.01	0.56	0.31	1.04
351.2	20.5	17.2	32.04	-3.15	0.29	0.95
350.0	61.5	17.4	53.57	-1.09	0.54	4.10
350.2	61.0	16.8	52.96	3.22	0.56	4.30
351.2	60.5	17.3	38.82	0.10	0.48	4.03
350.0	61.0	17.0	42.26	-3.34	0.49	4.46
399.7	20.5	16.7	72.80	16.92	1.11	5.04
400.2	20.5	17.0	75.90	16.63	1.33	5.27
399.9	60.5	16.5	88.85	26.04	2.06	8.03
400.2	61.0	16.6	90.38	27.65	1.65	8.16

* Percent in recovered reaction solvent.
** NA= Not available.

Table 2. Results of the statistical analyses of operator 2's measured THF and heptane conversion data.

	THF Conversion (%)			HEPTANE Conversion (%)		
Parameter	Model Estimate	Meas'd Average	Std. Error	Model Estimate	Meas'd Average	Std. Error
Constant*	18.5		2.5	-2.9		1.0
Time	11.5		2.5	2.8		1.2
Temperature	33.6		3.5	17.5		1.5
Catalyst	16.6		3.1			
Time-Temp. Int.				7.5		2.0
Temp.-Cat. Int.	9.3		5.0			
Experimental Error	5.6			2.1		
350°C, 20min, 0%	18.5	20.1	2.5	-2.9	-3.0	1.0
350°C, 60min, 0%	30.0	27.0	2.4	-0.1	0.9	0.7
400°C, 20min, 0%	52.1	48.7	3.0	14.6	13.5	1.1
400°C, 60min, 0%	63.6	62.8	3.0	24.8	23.4	1.2
375°C, 40min, 0.5%	51.6	58.8	1.1	9.1	7.6	0.4
350°C, 20min, 1%	35.1	33.5	1.8	-2.9	-1.3	1.0
350°C, 60min, 1%	46.6	46.9	2.3	-0.1	-0.3	0.7
400°C, 20min, 1%	77.9	74.4	3.0	14.6	16.8	1.1
400°C, 60min, 1%	89.4	89.6	3.0	24.8	26.8	1.2
R^2	0.94			0.96		

* Value calculated for a thermal reaction at 350°C for 20 minutes with 1% sulfur addition.

Table 3. Results of the statistical analyses of operator 2's measured gas yields and DHP in the recovered solvent.

	GAS YIELD (%dmmf coal)			DHP (%)		
Parameter	Model Estimate	Meas'd Average	Std. Error	Model Estimate	Meas'd Average	Std. Error
Constant*	0.25		0.05	0.40		0.42
Time	0.23		0.07	0.40		0.46
Temperature	0.91		0.08	1.03		0.49
Catalyst				0.85		0.48
Time-Temp. Int.	0.43		0.11	0.52		0.49
Time-Cat. Int.				2.39		0.49
Temp.-Cat. Int.				2.83		0.48
Experimental Error	0.12			0.49		
350°C, 20min, 0%	0.25	0.30	0.05	0.40	0.33	0.42
350°C, 60min, 0%	0.48	0.52	0.04	0.80	0.62	0.24
400°C, 20min, 0%	1.15	1.20	0.06	1.43	1.07	0.32
400°C, 60min, 0%	1.82	1.90	0.06	2.35	2.31	0.32
375°C, 40min, 0.5%	0.92	0.78	0.02	2.97	3.78	0.11
350°C, 20min, 1%	0.25	0.30	0.05	1.25	0.99	0.32
350°C, 60min, 1%	0.48	0.52	0.04	4.04	4.22	0.23
400°C, 20min, 1%	1.15	1.22	0.06	5.10	5.16	0.32
400°C, 60min, 1%	1.82	1.86	0.06	8.41	8.10	0.31
R^2	0.96			0.96		

* Value calculated for a thermal reaction at 350°C for 20 minutes with 1% sulfur addition.

Table 4. Number of reactions completed by each operator for PNL's catalyst.

TARGET CONDITIONS			NUMBER OF REACTIONS	
TEMP. (°C)	TIME (min)	CATALYST (wt%)*	OPERATOR 1	OPERATOR 2
350	20	0	0	3
350	60	0	1	4
400	20	0	1	2
400	60	0	2	2
375	40	0.5	0	5
350	20	1	0	2
350	60	1	1	4
400	20	1	1	2
400	60	1	3	2

* Precursor based on as-received coal.

Table 5. Models for THF conversion without the 350°C, 20 minute experimental results.

	ESTIMATES (%)	
PARAMETER	OPERATOR 1	OPERATOR 2
Constant*	28.0	17.0
Time	12.0	11.9
Temperature	25.0	32.7
Catalyst	17.2	16.4
Temperature-Catalyst	6.2	9.5
Experimental Error	3.2	4.3

* Value calculated for a thermal reaction at 350°C for 20 minutes with 1% sulfur addition.

Table 6. Calculated results (400°C, 60 minutes).

	THF Conv. (%)	DHP (%)*
1wt%** PNL Cat. Precursor + 1wt%** Sulfur	89.4	8.41
Thermal + 1wt% Sulfur	63.6	2.35
1wt% U. of Pitt. Cat. Precursor + 2wt% Sulfur	82.3	5.35
Thermal + 2wt% Sulfur	63.0	2.43
1wt% Pyrite	73.4	3.88
Thermal	54.9	1.08

* Percent of recovered reaction solvent.
** Weight percents based on as-received coal.

SYNTHESIS AND CHARACTERIZATION OF NANOSCALE TRANSITION METAL NITRIDES AND CARBIDES FROM METALORGANIC AND HALOGENATED PRECURSORS

R.Ochoa[1], [2]P. Zhou, [2]W.T. Lee, [2]A. Rao, [4]S. Bandow, and [1,2] P.C. Eklund
[1]Center for Applied Energy Research, [2] Department of Physics and Astronomy,[3] Department of Materials Science and Engineering, University of Kentucky, Lexington KY 40506.[4] Instrument Center, Institute for Molecular Science, Myodaiji Okazaki, 444 Japan.

KEYWORDS: Laser Pyrolysis, molybdenum nitride, molybdenum carbide

INTRODUCTION

High surface area ultrafine particle catalysts offer a large number of advantages compared to conventional catalysts: no diffusion resistance, high accessibility of reactants to the active centers of the catalyst, and a large number of active sites per particle. In coal liquefaction, highly dispersed catalysts are especially needed because the catalyst particles are only able to influence reactions within their immediate vicinity .

Laser pyrolysis constitutes a new method for the preparation of ultrafine particle catalysts. This technique is a verstile non-equilibrium thermodynamic process for the production of nanoscale particles involving fast growth and rapid heating/cooling rates (10^5 °/s) which also allows the synthesis of metastable phases. The process involves a gas phase pyrolysis reaction, of two or more molecular species, sustained by the heat generated through the absorption of CO_2 laser energy into vibrational-rotational excitations of at least one of the reactant gas species. Typical reaction temperatures are estimated to be 800-1000°C. A variety of nanoscale particles have been produced using this technique and include MoS_2, WS_2, Fe_3C, Fe_7C_3 [1,2].

We have also prepared high surface area (50-86 m^2/g) Mo_2C and Mo_2N ultrafine particles (UFP) by Laser pyrolysis using $Mo(CO)_6$ as the metal precursor. Previously, Mo_2N and Mo_2C (100-200 m^2/g) have been produced by Temperature Programmed Reduction. This method consists in the reduction of MoO_3 by NH_3 [3,4] or a mixture of H_2/N_2[5] or CH_4/H_2[3] for Mo_2N and Mo_2C, respectively. It has been reported that these materials exhibit high activity for heteroatom removal in the hydrotreatment of naphtha and upgrading of coal liquids [6] .

Mo_2C and Mo_2N are interstitial alloys formed by the incorporation of carbon, nitrogen and oxygen into the lattice of Mo metal . In these materials, the non-metallic elements (C, N, O) enter into the interstitial sites between metal atoms. Since the bonding among those light elements is very similar, carbonitrides, oxynitrides and oxycarbide phases are possible, depending on the conditions of synthesis [7].

The ability of these materials to incorporate oxygen into their structure is particularly important with respect to their catalytic properties since it has been demonstrated that oxygen together with carbon deposits seriously decrease and/or modify their activity. Therefore it is important to address the nature of the surface of these catalysts as well as to be able to prepare these materials in an oxygen free (or controlled oxygen content) and amorphous carbon free form. For this reason, the role of the precursor and the conditions of preparation are very important.

Several reports have been presented in the literature regarding the effect of chemisorbed oxygen, surface oxide or even intercalated oxygen on the catalytic properties of these materials [8-11] . In these sudies, it has been suggested that a certain amount of oxygen in the catalyst may confer a double functionality: that of a lewis acid as well as of a noble metal [8,10].

This work contains the results from the structural and chemical characterization of Mo_2N and Mo_2C UFP catalysts by X-ray diffraction (XRD) , scanning tunneling microscopy (STM), x-ray photoelectron spectroscopy (XPS) and thermogravimetry-mass spectrometry (TG-MS). The main objectives are to elucidate the real composition and surface state of these nanoparticles, to correlate structure and composition with catalytic properties and to determine methods to synthesize them in an oxygen-free and carbon- free form.

EXPERIMENTAL

Details from the experimental apparatus and procedure have been reported elsewhere [1]. Briefly, nanoscale Mo_2N and Mo_2C were synthesized from the reaction of $Mo(CO)_6$ in the presence of ammonia or ethylene. The catalysts were passivated in a flow of 5% O_2/ He for several hours before removal from the reaction chamber.

Mo_2C was also synthesized utilizing $MoCl_5$ as the metal precursor with the same synthesis parameters that were used for the carbonyl precursor . Table 1 summarizes the reaction conditions employed to synthesize these phases. Notice that the yield of Mo_2C synthesized from $MoCl_5$ is lower than when $Mo(CO)_6$ is used.

TABLE 1

Synthesis Parameters	Mo_2C	Mo_2N	Mo_2C
Laser Intensity	95W	95W	95W
Chamber Pressure (Torr)	200	200	200
Metal Precursor	$Mo(CO)_6$	$Mo(CO)_6$	$MoCl_5$
Reactant Gas	C_2H_4	NH_3	C_2H_4
Flow rate (sccm)	80	118	80
Temperature (sublimation cell)	105°C	105°C	150°C
Yield (g product/g precursor)	1.5g/5g	1.5g/5g	50 mg/2 g

CHARACTERIZATION

X-Ray Diffraction

X ray diffraction was used to identify the crystalline phase of the particles as well as to extract average values of the lattice spacing and of the crystallite size of the nanoscale particles. X-ray data were collected using Cu ($K\alpha$) radiation using a Philips 3100 powder diffractometer. The average particle diameter was estimated from the Debye-Scherrer (DS) equation $D=0.9\lambda/A\cos(\Theta_{111})$ [12]. Figure 1 presents the X-ray diffraction data obtained from a Mo_2C UFP. The phase of this carbide has been identified as fcc Mo_2C. The crystallite size calculated for this materials is 2.1 nm which is in good aggreement with the value obtained using HRTEM [12].

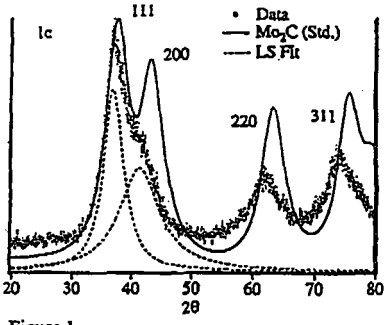

Figure 1
X ray diffractogram of Mo_2C

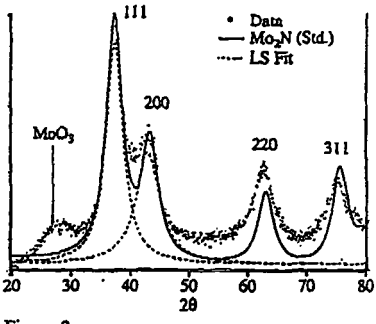

Figure 2
X-Ray diffractogram of Mo_2N

The solid lines in figure 1 correspond to the data generated using a Lorentzian lineshape for the diffraction peaks and an exponential term for the background. The values used for the diffraction peak positions and peak areas were taken from a standard powder diffraction file. The difference in intensities between the standard powder diffraction and the data may be attributed to Mo vacancies in the crystalline structures of the particles or to variations in the metal atom sublattice near the surface. Clear shifts of the diffraction lines toward lower 2Θ angles is seen for Mo_2C. This indicates a lattice expansion, presumably associated with the small crystallite size. Figure 2 presents the X-ray diffraction data for Mo_2N which has been identified as fcc Mo_2N. These particles showed an average crystallite size of 2.5 nm.

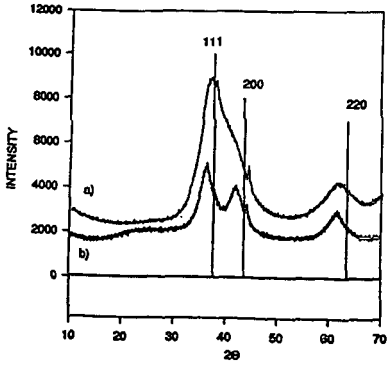

Figure 3
X-ray diffractograms from a) Mo_2C synthesized from $Mo(CO)_6$ and b) Mo_2C synthesized from $MoCl_5$.

Figure 3 shows the x-ray diffraction data of Mo_2C synthesized using $MoCl_5$. The particle size calculated using the DS equation is 2.4 nm. Notice that now the peaks around $2\theta = 37.7°$ are well resolved and that no sign of $MoCl_5$ is present. The broad shoulder at $2\theta \sim 25°$ is attributed to the presence of a layer of MoO_3 [2]. High resolution TEM does not show any sign of oxide or carbide coatings. In particular the Mo_2C particles do not appear to have a carbon coating on the surface.

STM

The morphology of atomically flat Au(111) surfaces coated with mono- and multi-layer nanoscale Mo_2N particles was studied using a vacuum STM ($P<10^{-8}$ torr). The gold substrates were prepared by melting gold wires (0.5 mm diameter) in an acetylene/oxygen flame. These substrates exhibited large atomically flat areas with dimensions of about 100x100 $Å^2$ and terraces with single atomic step of approximately 2.4 Å. The particles were first dispersed in pentane or water solvent. Then they were sonicated for several hours and spin-coated onto the gold substrates. Heat treatment to remove adsorbed water and surface oxide was done in a sample-preparation chamber with a 100 torr of 10% H_2/He mixture. The STM image taken with a Pt/Ir tip is shown in figure 4.

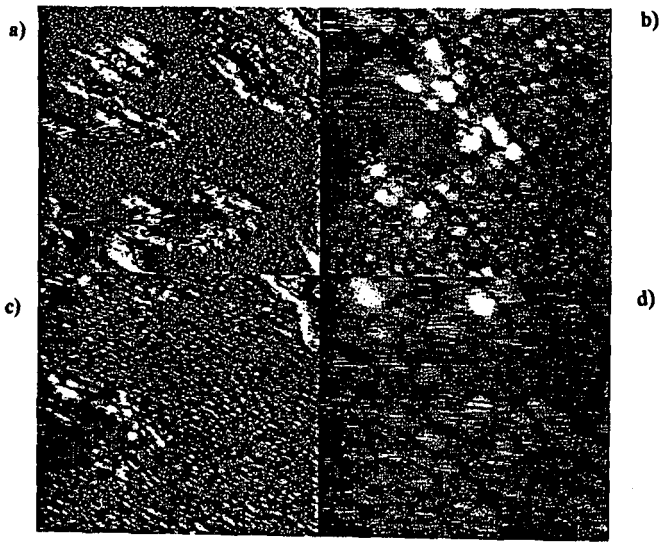

Figure 4
STM images of a layer of Mo2N UFP deposited on the surface of Au (111) at different magnifications. Each frame corresponds to an area of a)8000x8000 $Å^2$ b) 2000x2000 $Å^2$ c) 4000x4000 $Å^2$ d) 1000x10000 $Å^2$.

It is observed that a monolayer of nanoparticles has been deposited. The underlying terraces of Au(111) can still be observed (Figure 4a). The average particle size deduced from these images is ~ 7 nm. This value is higher than the one observed by TEM, probably because these particles correspond to a different batch from the one used to measure the TEM .

X-Ray Photoelectron Spectroscopy (XPS)

The XPS measurements were performed on a Leybold-Hereaus EA-11 spectrometer using Mg K- α (1253.6 eV) radiation at 15 kV and 20 mA. The oxygen/helium -passivated samples were prepared by pressing the powder into 13 mm diameter pellets. Figure 5 shows the XPS spectra from samples of Mo_2C and Mo_2N that were passivated in oxygen prior to their removal from the laser pyrolysis chamber. Figure 5a corresponds to the photoelectron lines of molybdenum $3d_{5/2}$ and $3d_{3/2}$ from Mo_2N , and figure 5b to the carbon 1s line from the same sample. Figures 5c and 5d correspond to the molybdenum and carbon peaks, respectively, from Mo_2C . The peaks at 228.58 eV in figures 5a and 5c have been assigned to the C-Mo and N-Mo bonding energies, whereas the ones at 232.2 eV to the +VI oxidation state of molybdenum , consistent with the presence of MoO_3 [13,14]. Deconvolution of the data gives 90% of surface molybdenum in the form of oxides (mainly MoO_3) for both Mo_2N and Mo_2C.

The carbon 1s peak in figure 5b, located at 284.5 eV is from carbon pressumably formed

during synthesis. No evidence was found of the presence of a carbidic surface phase in the molybdenum nitride sample. Deconvolution of the carbon photoelectron line from the molybdenum carbide sample gives two peaks at 283.7 eV and 284.5 eV which correspond to a mixture of carbidic carbon and amorphous carbon [13].

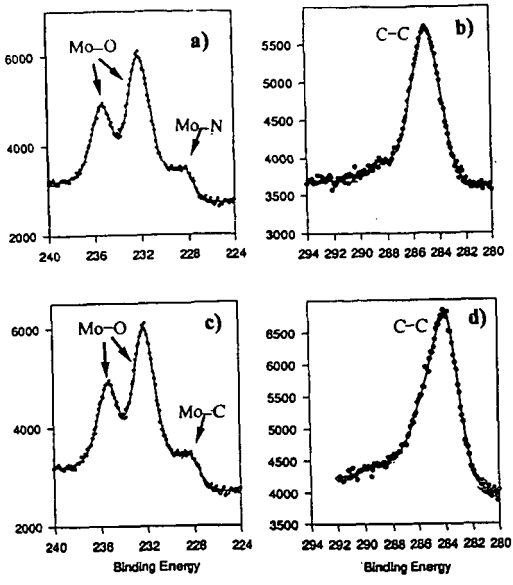

Figure 5
XPS data of Mo_2N and Mo_2C synthesized from the decomposition of $Mo(CO)_6$

Thermogravimetry-Mass Spectrometry (TG-MS)

Mo_2C and Mo_2N synthesized from the decomposition of $Mo(CO)_6$ were also studied with TG-MS. This technique provided valuable information about the surface composition and the extent of oxygen present on the catalyst. Between 5 and 7 mg of fresh catalyst (Mo_2N or Mo_2C) were loaded on the TG system and were flushed with He at room temperature for about 30 minutes. Pure He, and He mixed with 50% hydrogen were used as carrier gases in these experiments. The temperature program consisted on heating the samples from room temperature to 100°C. The samples were maintained at this temperature for 5 minutes, then they were heated to 900°C at a constant rate of 1°C/s . During the temperature ramp, the composition of the gas leaving the TG was monitored using a mass spectrometer.

Figure 6 shows the TG trace together with the mass signal from Mo_2C reduced in hydrogen. It is observed that there are three regions of weight loss in this sample. The first region at about 2 minutes (100°C) corresponds to the desorption of adsorbed water on the material. In the second temperature region from 8 to 12 minutes (200-410°C), oxygen is being removed from the sample in the form of water. The desorption of water occurs in the form of a broad peak that starts at about 200°C and which has a maximum at 540°C. There is still some water desorbing simultaneously with CO at a temperature about 620 °C . The presence of CO indicates that some oxygen from the sample is reacting with carbon from the material. At about 540°C carbon is being removed from the sample in the form of CH_4 with a maximum removal at 740°C. Notice also that after 18 minutes (800°C) , water continues to desorb indicating that even at this temperature oxygen has not been completely removed from the samples. Oxygen desorbed in the form of water below 500°C has been assigned to surface oxygen and near-surface oxygen [15] whereas that desorbed above that temperature has been assigned to the removal of deeper lying oxygen that has diffused from the particle interior to the surface.

In figure 7 the TG trace from Mo_2N is presented. This catalyst experienced a total weight loss of about 25%. Most of it comes from oxygen removal in the form of water. The water evolved at temperatures below 340°C has been assigned to surface oxygen and near-surface oxygen whereas water evolved above this temperature has been assigned to bulk oxygen. Although no ammonia was detected in the gases evolved, it is observed that at about 800°C the nitride decomposes by losing molecular nitrogen. Since no methane evolved from the heat treatment of Mo_2N , it follows that the methane detected from the carbide corresponds to carbidic carbon that has reacted with hydrogen, and that amorphous carbon was not removed

from the sample. This aggrees with reports that this carbon is very difficult to remove [15].

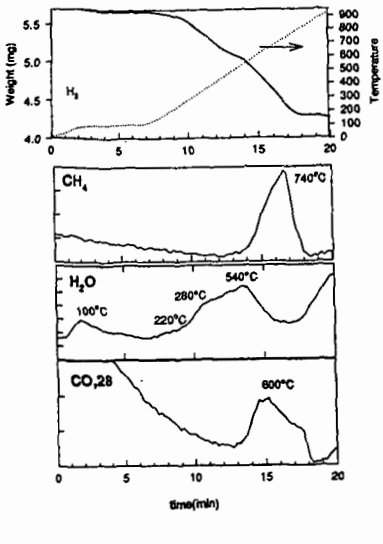

Figure 6
TG-MS trace of Mo_2C treated hydrogen

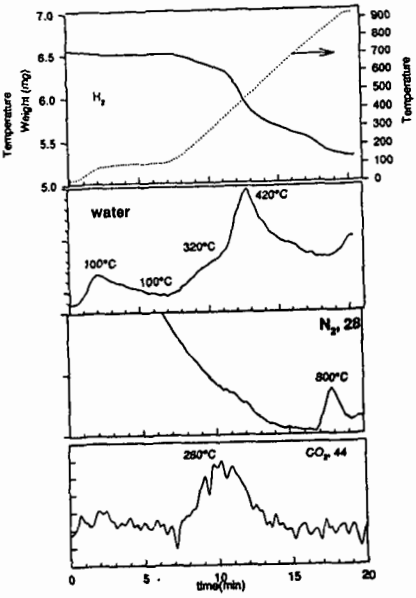

Figure 7
TG-MS trace of Mo_2N treated in hydrogen.

CONCLUSIONS

Fcc Mo_2N and Mo_2C have been synthesized from the decomposition of $Mo(CO)_6$ and $MoCl_5$ using Laser Pyrolysis. From the structural point of view, they appear crystalline with little or no disorder. Even though HR-TEM did not show any sign of oxide or carbide coating on the particle, XPS indicated that a large percentange of Mo atoms on the surface are in the form of an oxide phase produced during surface passivation. In addition, carbon was observed to be present on the surface of both catalysts from the decomposition of the metalorganic precursor. TG-MS shows that oxygen content constitutes a major contaminant on these particles and that polymeric carbon is very difficult to remove.

REFERENCES

[1] X.X. Bi, B. Ganguly, G.P. Huffman, F.E. Huggins, M. Endo, P.C. Eklund, J. Mater. Res. 8(7), (1993) 1666.

[2] X.X. Bi, Y. Wang, W.T. Lee, K.A. Wang, S. Bandow and P.C. Eklund, Mat. Res. Soc. Symp. Proc., 327, (1994) 47-52.

[3] S.T. Oyama, J.C. Schlatter, J. Metcalfe, J. Lambert , Ind. Eng. Chem. Res. 27, (1988) 1648-1653.

[4] J.-G. Choi, R. L. Curl, L.T. Thompson, J. of Catal. 146, (1994) 218-227.

[5] R.S. Wise, E.J. Markel, J. of Catal. 145, (1994) 344-355.

[6] S.T. Oyama, R. Kapoor, C. Shudakar, Prep. of Am. Chem. Soc. Div. Fuel Chemistry, 37(1), (1992) 233.

[7] S.T. Oyama, Catalysis Today, 15 (1992) 179-200

[8] H.S. Kim, G. Bugli, G. Djega-Mariadassou, Proc. Mater. Res. Soc. Symposium T, Nov 29-Dec. 1 1994.

[9] M. Ledoux, Proc. Mater. Res. Soc. Symposium T, Nov. 29-Dec 1 1994.

[10] F. H. Ribeiro, R.A. Dalla Betta, M. Boudart, J. Baumgartner, E. Iglesia, J. of Catal. 130, (1991)86-105.

[11] G.S. Ranhotra, A.T. Bell, J.A. Reimer, J. of Catal. 108, (1987) 40-49.

[12] X.X. Bi, K.D. Chowdhury, R. Ochoa, W.T. Lee, S. Bandow, M.S. Dresselhaus, P.C. Eklund in Proc. of Materils Res. Society Symposium T, Fall 1994, in press.

[13] M. J. Ledoux, C.P. Huu, J. Guille, H. Dunlop, J. of Catal., 134, (1992) 383.

[14] C.D. Wagner, W.M. Riggs, L.E. Davis, J.F. Moulder, and G.E. Muilenberg in " Handbook of X-ray Photoelectron Spectroscopy". Perkin-Elmer, Eden Prairie, MN, 1979.

[15] K.J. Leary, J. N. Michaels, A.M. Stacy, J. of Catalysis 101, (1986)301-313.

PROGRESS IN THE DEVELOPMENT AND PRODUCTION OF NANOSCALE IRON-CONTAINING CATALYSTS

Dean W. Matson, John C. Linehan, John G. Darab, Heather M. Watrob,
Eddie G. Lui, Max R. Phelps, and Michael O. Hogan
Pacific Northwest Laboratory[1]
PO Box 999
Richland, WA 99352

Keywords: iron-based catalysts, nanocrystalline catalysts, hydrothermal synthesis, model compounds

INTRODUCTION

The development of effective iron-based powders for use as dispersed catalysts or as precursors to the active catalyst phase in direct coal liquefaction processes is an ongoing area of research.[2-4] Although they are generally catalytically inferior to the more expensive catalyst materials based on molybdenum, cobalt, or nickel, iron-based powders offer the distinct advantages of relative low cost and toxicity. These factors make the prospects for using iron-based powders as one-time "throw away" catalysts attractive for large scale liquefaction operations since the costs associated with catalyst recovery could be avoided. Recent efforts have been aimed at increasing the efficiency of iron-based materials for coal liquefaction applications. Research has been focused on the development of ultrafine powders having very high specific surface areas and high dispersion in liquefaction media,[4] and on the effect of iron oxyhydroxide phase toward conversion of precursors to the active catalyst phase under liquefaction conditions.[5]

At the Pacific Northwest Laboratory (PNL) we have undertaken a program to investigate nanocrystalline iron-based powders as catalytic precursors in a variety of hydrocracking reactions, including coal liquefaction. One ultrafine powder synthesis method developed at PNL, the Rapid Thermal Decomposition of precursors in Solution (RTDS) process, appears to be particularly promising for use in the large scale production of nanocrystalline powders.[6,7] Using model compounds we have demonstrated that iron-based RTDS powders can be used to produce highly active carbon-carbon bond scission catalysts under reaction conditions relevant to coal liquefaction processes.[7,8] In this paper we present recent results of attempts at modifying the activity of RTDS-generated iron-based catalyst powders by doping with other metals and the results of scale-up efforts to produce kilogram quantities of active catalyst precursor by this process.

CATALYST PRECURSOR POWDER SYNTHESIS

When operated with an aqueous solvent, the RTDS powder synthesis method can be described as a continuous flow-through hydrothermal process. It involves the formation of ultrafine solid particles when homogeneous pressurized solutions are rapidly forced through a heated small diameter linear reactor (1-30 sec residence time). Under these conditions, well-known hydrothermal reactions, leading to nucleation of solid oxides or hydroxides, occur between dissolved metal species and the solvent.[9] Particle growth is quenched at the end of the reactor by passing the RTDS solution through an orifice, abruptly removing it from the hydrothermal environment. RTDS products are collected as aqueous suspensions in a cooled vessel, and typically contain submicrometer-sized aggregates of nanometer-sized crystallites. The solid powders can be separated from the suspension by centrifugation, spray drying, or freeze drying. Details of the RTDS process have been presented elsewhere.[6-8]

PNL currently has two operational RTDS units. One of these is referred to as a bench-scale unit and is used primarily for quick response feasibility studies and small batch (1-10 liters of precursor solution) sample processing. The reactor tube in this unit consists of a 1 to 2 meter length of 1/8 inch O.D. stainless steel high pressure tubing. Typical feedstock consumption rates and reaction residence times are 50-75 cc/min and 1-5 sec, respectively. The second RTDS system is referred to as an engineering-scale unit and has a larger reactor volume (with residence times of 5-30 sec) and greater throughput capacity (150-250 cc/min). In this system the reactor tube is a 2.25 meter length of 9/16 inch O.D. high pressure stainless steel tubing. The engineering-scale unit is used exclusively for runs involving greater than 10 liters of precursor solution.

While a range of iron-based oxide and oxyhydroxide phases can be produced using the RTDS method, we have targeted one phase, 6-line ferrihydrite,[10] as a candidate for large scale production as a coal liquefaction catalyst precursor. Preliminary tests have shown that this phase is consistently active as a liquefaction catalyst precursor,[5,8] and that it is particularly amenable to preparation using the RTDS method. Although 6-line ferrihydrite can also be produced using standard laboratory synthesis methods,[11] these are batch processes that are not necessarily scalable to larger batch sizes. Furthermore, benchtop 6-line ferrihydrite synthesis requires a time consuming dialysis step that can be eliminated by using the continuous RTDS method. We have investigated enhancing the rate of 6-line ferrihydrite production on the engineering-scale RTDS unit by increasing the iron salt content in the feed solution from 0.1 M to as high as 0.5 M.

In addition to single phase metal oxides and oxyhydroxides, mixed or doped oxide/oxyhydroxide powders are easily produced by the appropriate choice and loadings of dissolved solute in the RTDS feed solution. We evaluated the RTDS method for making 6-line ferrihydrite doped with 10

mole percent or less of an additional metal using the bench-scale RTDS apparatus. All doped 6-line ferrihydrite samples were prepared using a 0.1 M ferric nitrate solution as the iron source, and urea (0.5 M) was added to the feed solution to raise the pH of the solution in the hydrothermal region. RTDS reaction temperatures used were 300±5°C. The source of dopant metal ion and its nominal concentration in the feed solution are summarized in Table 1.

Unless otherwise noted, catalytic activities of all 6-line ferrihydrite powders reported in this work were evaluated using samples that had been separated from suspension by centrifugation, dried under flowing nitrogen, and ground and sieved to -325 mesh. Selected samples were calcined in air at 300°C for one hour. Catalytic evaluation of sample powders was undertaken by monitoring consumption of the model compound naphthylbibenzylmethane (NBBM) under a standard set of conditions. These tests were performed in sealed tubes containing 25 mg of NBBM, 100 mg of 9,10-dihydrophenanthrene, 3 mg catalyst precursor and 3 mg of sulfur. The tubes were suspended for 1 hr in a sand bath at the desired reaction temperature. Phase analyses of RTDS products were performed using powder X-ray diffraction (XRD) and metal contents were analyzed by inductively coupled plasma/mass spectrometry (ICP/MS).

RESULTS AND DISCUSSION

The catalytic activity of RTDS-generated undoped 6-line ferrihydrite toward the consumption of NBBM is shown in Figure 1. The 6-line ferrihydrite catalyst precursor was ground and sieved, and the -325 mesh fraction was calcined at 300°C for 1 hr prior to these tests. This figure clearly illustrates the high catalytic activity of this precursor phase at 400°C, consuming essentially all of the model compound at that temperature. Furthermore, moderate activities were retained to reaction temperatures as low as 300°C, where 30 percent of the model compound was consumed during a one hour reaction time.

ICP/MS analysis of powders produced by co-precipitation of iron and a second metal species in the presence of added urea using the bench-scale RTDS unit confirmed the usefulness of the RTDS technique for generating doped products of well-defined compositions (Table 1). XRD analysis of the doped powder products confirmed that 6-line ferrihydrite was the primary crystalline phase present in the products. A minor hematite component was also detected in the tin-doped powder product.

In general, the greatest discrepancies between the nominal dopant contents in the RTDS feed solutions and the measured dopant contents of the dried powders were found in the samples having the smallest dopant contents (1 mole percent dopant metal). The primary source of these discrepancies most likely resulted from uncertainties in weighing the dopant salts when preparing the RTDS feed solutions. The analytical results on the doped ferrihydrite products indicate that essentially all of the iron and the dopant metal present in the feel solutions are precipitated in the RTDS unit and that doping levels closely follow the feed concentrations. This suggests that the RTDS process could be very valuable for the co-processing of semi-precious or precious metal catalysts on supports or, as in this case, the production of co-catalysts. The fine control over doping levels exhibited by the RTDS process has important prospective applications beyond coal liquefaction catalyst production. Many different catalysts are mixtures of two or more active species where the exact composition is important to promote both increased reactivity and lower costs. In RTDS experiments with zirconia as the major product constituent similar doping results have been obtained.

Catalyst testing results measuring consumption of the NBBM model compound using the doped 6-line ferrihydrite powders as catalyst precursors are presented in Figure 2. The result of catalyst evaluation of an undoped RTDS 6-line ferrihydrite powder produced under comparable conditions is presented for comparison. When using the centrifuged, dried, and sieved powders as catalyst precursors without calcination (Fig. 2), NBBM consumptions approaching 90 percent and above were observed for chromium, zirconium, and molybdenum doped powders. Cobalt and nickel doped 6-line ferrihydrite products exhibited a range of intermediate to poor activities with the 10 percent nickel product consuming less than 20 percent of the model compound. The tin-doped product that was tested exhibited no apparent activity toward consumption of NBBM whatsoever. We speculate that this was due the presence of residual chlorine (a known catalyst poison) from the salt used as the source of tin ions in the RTDS solution.

XRD analysis of the samples calcined at 300°C for 1 hr indicated that ferrihydrite remained the predominant phase after calcination. Those uncalcined samples exhibiting strong catalytic activity all lost less than 15 percent of their weight upon calcination while those with low activity lost up to 30 percent of their weight, most likely due to adsorbed water. The presence of excess adsorbed water may be detrimental to catalytically enhanced C-C bond scission reactions in the test system. An additional point can be made, however, that loadings of catalyst precursor samples containing excess adsorbed water would contain a correspondingly lower metals content, potentially reducing the measured catalytic activity per unit mass of catalyst precursor powder.

Calcination of the doped 6-line ferrihydrite samples produced a significant improvement in the measured catalytic activities of samples having mediocre activities in the uncalcined state (Fig. 2). Upon calcination, two of the cobalt doped powders consumed more than 90 percent of the model compound. The 10 percent nickel doped sample showed significant improvement as a result of calcination, increasing from less than 20 percent to nearly 70 percent consumption of the NBBM. Those powders previously exhibiting high activity retained that activity after calcination and no

improvement was noted in the activity of the tin doped sample. The undoped ferrihydrite sample also showed an increase in activity with calcination even though the weight loss was only 6 percent. The activity toward NBBM consumption increased from 68 percent to over 90 percent.

Undoped 6-line ferrihydrite powders were produced using the engineering-scale RTDS reactor at increasing RTDS reaction temperatures to evaluate the effects of this variable using a constant 0.1 M ferric nitrate/0.5 M urea feed solution. Product suspensions produced at increasing temperatures starting at 255°C and increasing to 315°C were split into two fractions, one centrifuged and dried as summarized above, and the other spray dried in a bench-scale spray drying unit. Both splits were calcined at 300°C before catalyst testing. When evaluated for catalytic activity (Fig. 3) all of the centrifuged samples promoted NBBM consumptions in excess of 90 percent. Spray dried samples of the same products were generally somewhat inferior catalysts, likely resulting from incorporation of water soluble salts into the spray dried powders. This incorporation of salts in the powder could cover some percentage of the otherwise available catalytic sites and would also reduce the effective metal content per gram of catalyst powder. If spray dried RTDS products are to be used for coal liquefaction applications, catalyst loadings may be required to compensate for this effect.

Efforts at increasing the production rate of 6-line ferrihydrite powders with the engineering scale unit were focused on use of higher concentrations of ferric ion in the feed solution. Ferric nitrate concentrations ranging from 0.1 M to 0.5 M with a constant urea-to-Fe^{3+} ratio of 5:1 were used as feedstocks for these experiments. At the flow rates of the RTDS unit the 0.5 M ferric ion concentration corresponded to a I lb of dried powder-per-hour rate of production. The catalytic activities of these powders, as a function of the production rate, before and after calcination are shown in Figure 4. Notice that there is little difference in the activity of the calcined and uncalcined powders up to the highest production rate. Powders produced at 0.8 lb/hr showed some of the highest catalytic activities measured for iron oxide powders.

SUMMARY

The RTDS powder synthesis method has been shown suitable for producing nanocrystalline 6-line ferrihydrite powders that are highly active as precursors to catalysts promoting carbon-carbon bond scission reactions in coal model compounds. Activity of the ferrihydrite powder is maximized if it is sieved to fine aggregate size and pretreated at 300°C prior to use as a catalyst precursor. This material has been shown to exhibit catalytic activity at reaction temperatures as low as 300°C. We have demonstrated the capability to generate the ferrihydrite powder product at rates of up to 1 lb/hr using an engineering-scale RTDS unit. The method has also been demonstrated to be capable of producing ferrihydrite powders accurately doped with a second metal component that may modify the catalyst characteristics.

ACKNOWLEDGMENTS

This work was supported by the U.S. Department of Energy, Office of Fossil Energy. Support for EGL and HMW was provided by the Associated Western Universities, Inc., Northwest Division under Grant DE-FG06-89ER-75522 with the U.S. Department of Energy.

REFERENCES

(1) Pacific Northwest Laboratory is operated for the US Department of Energy by the Battelle Memorial Institute under contract DE-AC06-76RLO 1830.
(2) Rabo, J.A., in *Advanced Heterogeneous Catalysts for Energy Applications Vol. II*, U.S. DOE report DOE/ER-30201-H1, **1994**, p. 1.1.
(3) Pradhan, V.R.; Tierney, J.W.; Wender, I.; and Huffman, G.P., *Energy and Fuels*, **1991**, 5, 497.
(4) Derbyshire, F., *Energy and Fuels*, **1989**, 3, 273.
(5) Linehan, J.C.; Matson, D.W.; and Darab, J.G., *Energy and Fuels*, **1994**, 8, 56.
(6) Matson, D.W.; Linehan, J.C.; Bean, R.M., *Materials Letters* **1992**, 14, 222.
(7) Darab, J.G.; Buehler, M.F. ; Linehan, J.C.; and Matson, D.W., in *Better Ceramics Through Chemistry VI*, Materials Research Society symposium proceedings vol. 346, Cheetham, A.K., Brinker, C.J., Mecartney, M.L., and Sanchez, C., eds. Materials Research Society, pp. 499-510.
(8) Matson, D.W.; Linehan, J.C.; Darab, J.G.; and Buehler, M.F., *Energy and Fuels*, **1994**, 8, 10.
(9) Rabenau, A., *Angew. Chem., Int. Ed. Engl.*, 1985, 24, 1026.
(10) This weakly crystalline iron oxyhydroxide phase is named for the number of broad lines present in its powder XRD pattern.
(11) Schwertmann, U. and Cornell, R.M., *Iron Oxides in the Laboratory*, Weinheim; New York, 1991.

Table I. Iron Oxides Doped with Transition Metals Produced by Co-Processing a Second Metal Salt and 0.1 M Ferric Nitrate using RTDS

Dopant Salt	Nominal Mole Percent Dopant Metal in Feed	Measured Mole Percent Dopant Metal in Isolated Powder	Percent Difference Between Feed and Powder	Phases Detected by XRD
Cobalt Acetate	10	9.27	7	6-line Ferrihydrite
Cobalt Acetate	1	1.11	11	6-line Ferrihydrite
$Ni(NO_3)_2$	10	9.82	2	6-line Ferrihydrite
$Ni(NO_3)_2$	1	1.21	21	6-line Ferrihydrite
$SnCl_2$	1	1.10	10	6-line Ferrihydrite/ Hematite
$Cr(NO_3)_3$	10	9.89	1	6-line Ferrihydrite
$Cr(NO_3)_3$	1	1.23	23	nd
$ZrO(NO_3)_2$	10	9.36	6	6-line Ferrihydrite
$(NH_4)_2MoO_4$	1	0.98	2	6-line Ferrihydrite

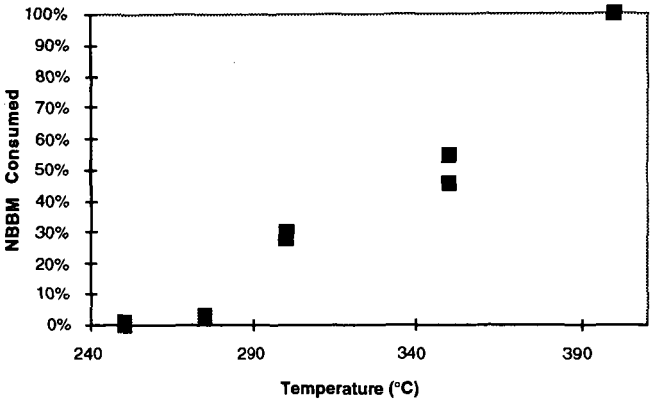

Figure 1. Effect of reaction temperature on catalytic activity of undoped RTDS-generated 6-line ferrihydrite toward consumption of NBBM model compound.

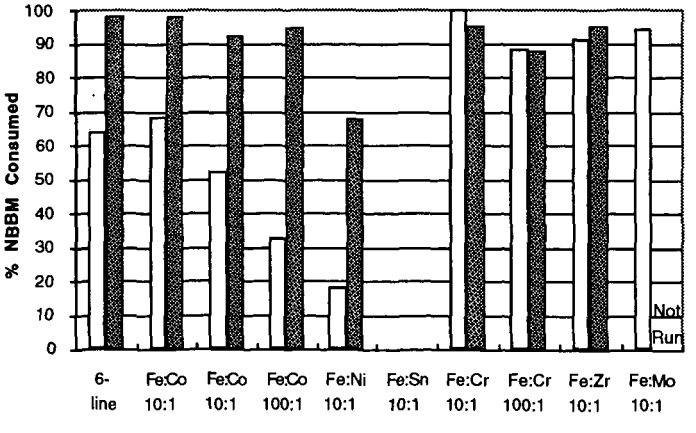

Figure 2. Effect of calcining at 300°C for one hour on activity of RTDS-generated 6-line ferrihydrite and doped 6-line ferrihydrite powders toward consumption of NBBM model compound at 400°C. All samples were sieved to -325 mesh. Unshaded bars represent uncalcined powders, shaded bars represent calcined powders.

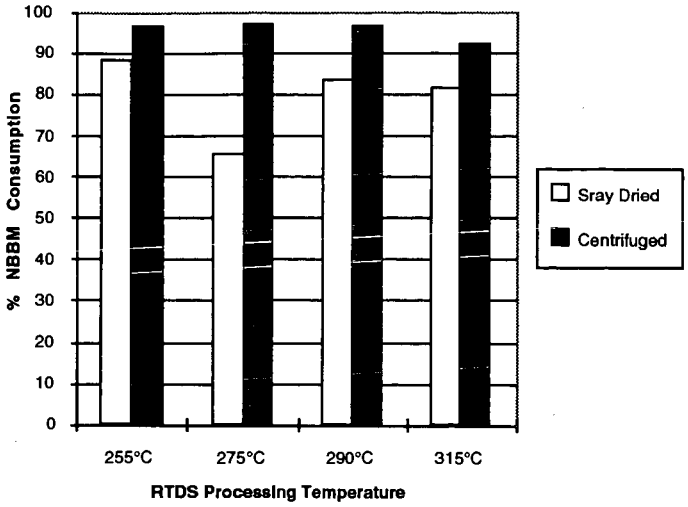

Figure 3. Effect of engineering-scale RTDS temperature and collection method on measured catalytic activity of calcined 6-line ferrihydrite powder toward consumption of NBBM model compound.

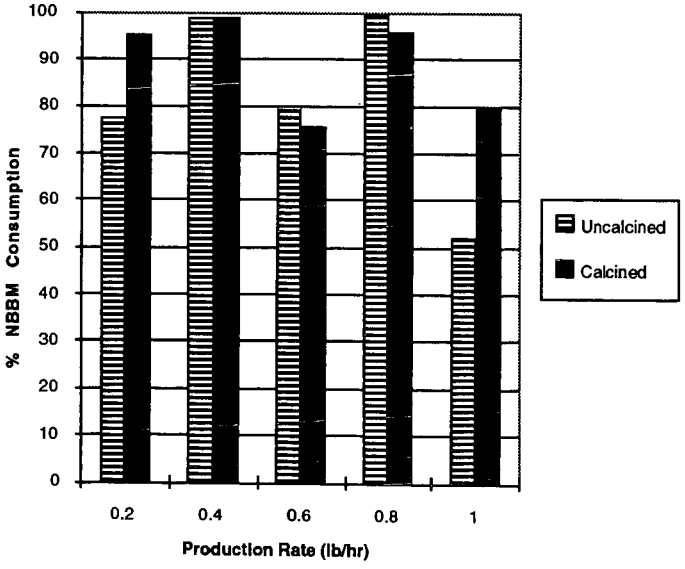

Figure 4. Activities of calcined and uncalcined 6-line ferrihydrite powders produced on the engineering-scale RTDS apparatus at increasing production rates.

CHARACTERIZATION OF $Fe_{1-x}S$ CATALYSTS SYNTHESIZED FROM FERRIHYDRITES UNDER DCL CONDITION

Jianmin Zhao, Zhen Feng, Frank E. Huggins, K. R. P. M. Rao, and Gerald P. Huffman*
The Consortium for Fossil Fuel Liquefaction Science
341 Bowman Hall, University of Kentucky
Lexington, KY 40506

Keywords: Pyrrhotite catalysts; direct coal liquefaction; Mossbauer spectroscopy; XRD; TEM.

INTRODUCTION

Recently, considerable effort has been made to develop low cost, highly dispersed iron-based catalysts for direct coal liquefaction (DCL) [1]. Most iron-based catalysts are in fact the catalyst precursors as the catalysts convert to $Fe_{1-x}S$ (pyrrhotite) under DCL reaction conditions. There has been less work reported on the pyrrhotite phase, in terms of its morphology and structure, and how they influence DCL activity.

In the past, we have extensively investigated the structure and DCL activity of ferrihydrite (FHYD), a highly dispersed iron oxide with surface area >200 m^2/g and average particle size of 30-50 Å. The major drawback of this material as a catalyst is that the small particles quickly agglomerate and transform to a low surface area hematite (α-Fe_2O_3) at T > 200°C. Moreover, the presence of surface adsorbed water molecules accelerates the agglomeration and phase transformation [2, 3]. This problem has been resolved by chemisorption of small amounts of impurity anions at the surface of ferrihydrite. The impurity anions block the crystal growth sites and thereby effectively inhibit the phase transformation to hematite, allowing the catalyst to maintain its dispersion. A number of binary ferrihydrite catalysts (M/FHYD, M/Fe ≈ 5%) with M = Si, Mo, P, and citric acid (CA) have been synthesized in our laboratory [4, 5]. DCL tests using Si/FHYD and CA/FHYD show significant increases of coal→liquid conversion over that obtained from thermal reaction, or with pure ferrihydrite [4, 5].

In this paper, we report the characterization of pyrrhotite catalysts synthesized under simulated DCL conditions using binary ferrihydrites as the catalyst precursors. TEM, XRD, and Mössbauer spectroscopy were used for the characterization.

EXPERIMENTAL

Three ferrihydries were used: a pure ferrihydrite catalyst (30-Å catalyst) provided by Mach I, Inc., and two binary ferrihydrites Si/FHYD and CA/FHYD synthesized in our laboratory. Details of the synthesis can be found in Ref. 4 and 5.

Sulfidation of the catalysts was performed in a tubing bomb under simulated DCL conditions. The tubing bomb was loaded with 0.25 g of catalyst mixed with tetralin along with dimethyl disulfide (DMDS) as a sulfur donor (S/Fe = 2/1, by weight). The tubing bomb was than pressurized with H_2 to 1000 psi at room temperature and agitated vertically at 400 cycles/min in a fluidized sand bath at 415 °C for one hour. After reaction, the samples were subjected to XRD, TEM and Mössbauer investigation.

Mössbauer spectra were recorded using a constant acceleration spectrometer. The radioactive source consists of ~50 mCi of ^{57}Co in a Pd matrix. Powder X-ray diffraction (XRD) was performed on an automated Rigaku Dmax X-ray diffractometer. Transmission electron micrographs (TEM) were obtained with a Hitachi H800 NA scanning transmission electron microscope (STEM).

RESULTS AND DISCUSSION

TEM For the pure ferrihydrite (30-Å), after sulfidation, TEM shows the formation of well crystallized, hexagonal-shaped $Fe_{1-x}S$ particles with average particle size > 1000 Å (Fig. 1). Similar result has been reported previously by Srinivasan et al [6]. Improved dispersion of the $Fe_{1-x}S$ phase is obtained with the binary ferrihydrites as indicated in Fig 1, showing significantly smaller particles of less regular shape.

X-ray diffraction $Fe_{1-x}S$ has the NiAs structure in which each Fe is surrounded by six sulfur atoms, and Fe has 1, 2, or 4 vacancies among its 12 nearest Fe neighbors. The monoclinic (Fe_7S_8) and hexagonal (Fe_9S_{10}) phases are the most common ones. The phase transition of monoclinic to hexagonal occurs at ~300°C. The XRD patterns for the three ferrihydrite catalysts after sulfidation are consistent with those for the hexagonal phase (Fig. 2). However, the

pyrrhotite phase formed with Si/FHYD shows difraction features on the high 2θ sides of the major diffraction peaks, which are also seen in the monoclinic phase (Figure 2a, indicated by arrows). Because of decreased Fe:S ratio, the d spacing for the monoclinic phase is shorter than that for the hexagonal phase, thus the (102) peak for the monoclinic phase is shifted to higher 2θ. Such shifting is also found for the sulfided Si/FHYD and the 350°C sulfided 30-Å catalyst, indicating incomplete mono-hex transition, due to the presence of the surface adsorbed Si and lower sulfiding temperature, respectively. For reasons unclear at the present time, the (102) peak for the sulfided CA/FHYD is shifted to the low 2θ side.

Mössbauer spectra Quantitative analysis for the Fe vacancies in pyrrhotite are obtained using Mössbauer spectroscopy. The Mössbauer spectrum for the hexagonal phase contains three sextets with magnetic hyperfine fields of H_f = 302, 274, and 256 kOe, respectively [7]. These three components are assigned to three Fe positions, which respectively have 0 (position A), 1(B), and 2(C) vacancies among their Fe neighbors. For the monoclinic pyrrhotite, the spectrum also consists of three sextets of H_f = 300, 256, and 225 kOe, corresponding to the Fe atoms with 0 (A), 2(C), and 4(D) vacancies in their Fe neighbors. Figure 3 shows the Mössbauer spectra of the three pyrrhotite catalysts. The spectrum for the sulfided 30-Å catalysts is very similar to that for hexagonal phase, which is dominated by the A, B, and C positions. However, a fourth component (D) is discernable, hence the spectrum is fitted with four sextets. The spectrum for the sulfided Si/FHYD is similar to that for the monoclinic phase, showing splitting of the absorption lines, due to decreased population of the B position and increased population of the C and D positions. The spectrum is fitted with three sextets representing the A, C, and D positions, and a doublet at the center for the unsulfided ferrihydrite. The results are in agreement with the XRD results. The spectrum for the sulfided CA/FHYD also shows increased splitting of the absorption lines as compared with that for Si/FHYD, indicating increased fractions of the C and D components. The spectrum is fitted with four sextets. The Mössbauer parameters are listed in Table 1.

According to the distribution of the four magnetic components (Table 1), a measure of the vacancy content in the nearest Fe shell, V is given by

$$V = \frac{(m*1 + l*2 + k*4)}{(n + m + l + k)} \qquad (1)$$

where n, m, l, k represent the normalized fractions of four positions with 0, 1, 2, 4 vacancies, respectively. V values for the three samples are listed in Table 1. Significant increase of the Fe vacancies are found in the sulfided Si/FHYD and CA/FHYD.

In conclusion, we found that in addition to improving the dispersion of the pyrrhotite phases, the presence of impurity anions at the ferrihydrite surface retards the mono-hex phase transition, thus more Fe vacancies are retained in the pyrrhotite phase. The role of these Fe vacancies on catalytic coal liquefaction will be further investigated.

ACKNOWLEDGEMENT This research is supported by the U. S. Department of Energy under contract No. DE-FC22-90PC90029, as part of the research program for the Consortium for Fossil Fuel Liquefaction Science.

REFERENCES

1. Huffman, G. P. et al, *Energy & Fuels* **1993**, 7, 285.
2. Zhao, J.; Huggins, F. E.; Feng, Z.; Lu, F.; Shah, N.; Huffman, G. P. *J. Catal.* **1993**, 143,
3. Feng, Z.; Zhao, J.; Huggins, F. E.; Huffman, G. P. *J. Catal.* **1993**, 143, 510.
4. Zhao, J.; Feng, Z.; Huggins, F. E.; Huffman, G. P. *Energy & Fuels* **1994**, 8, 38.
5. Zhao, J.; Feng, Z.; Huggins, F. E.; Huffman, G. P. *Energy & Fuels* **1994**, 8, 1152.
6. Srinivasan, R.; Keogh, R. A.; Davis, B. H., preprint paper, *ACS Div. Fuel Chem.* **1992**, 37, 1265.
7. Ovanesyan, N. S; Trukhtanov, V. A., Ordinets, G. Yu.; Novikov, G. V., *Soviet Physics JEPT* **1971**, 33, 1193.

Table 1. Mössbauer parameters for the ferrihydrite catalysts after sulfidation without coal. *H* is for the magnetic hyperfine field; IS the isomer shift; QS the quadruple splitting. A, B, C, and D represent the Fe positions with 0, 1, 2, and 4 Fe vacancies among its Fe neighbors. The average vacancy is determined by Eqn. (1). All spectra were recorded at room temperature.

Sample	H (kOe)	IS (mm/s)	QS (mm/s)	Phase	% Fe	V
30-Å	297	0.69	0.06	A	30.9	1.22
	274	0.72	0.04	B	31.2	
	257	0.69	0.07	C	30.5	
	232	0.60	0.11	D	7.4	
CA/FHYD	296	0.69	0.05	A	32.3	1.35
	273	0.71	0.04	B	23.9	
	255	0.68	0.05	C	32.1	
	227	0.63	0.09	D	11.8	
Si/FHYD	294	0.68	0.05	A	30.0	1.59
	255	0.67	0.05	C	26.6	
	223	0.65	0.09	D	15.3	
		0.45	0.52	FHYD	28.0	

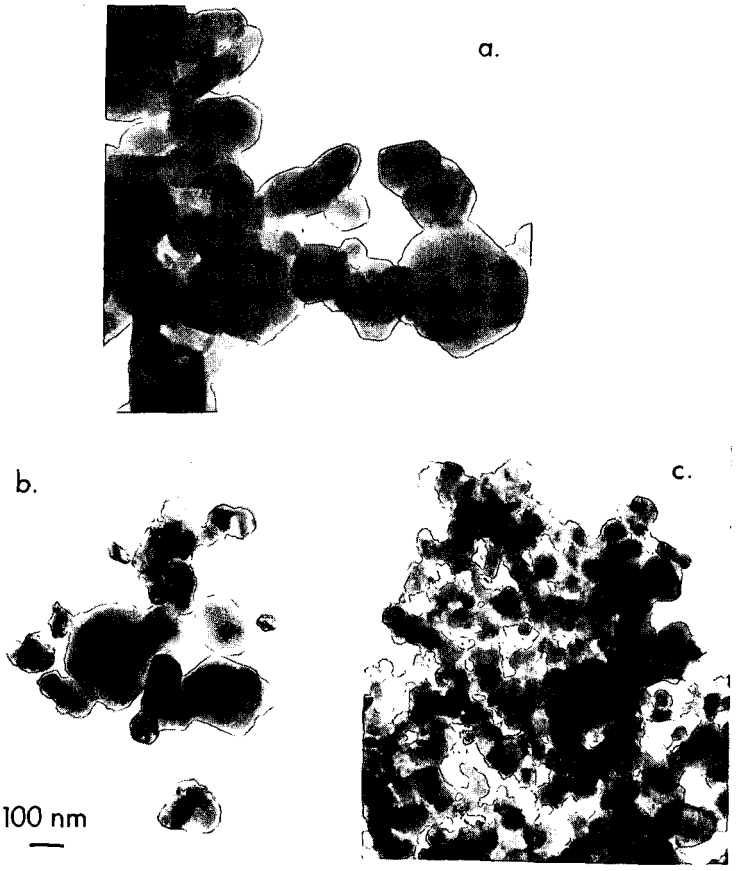

Figure 1 TEM for three sulfided ferrihydrites: a) the 30-A catalyst; b) CA/FHYD; c) Si/FHYD.

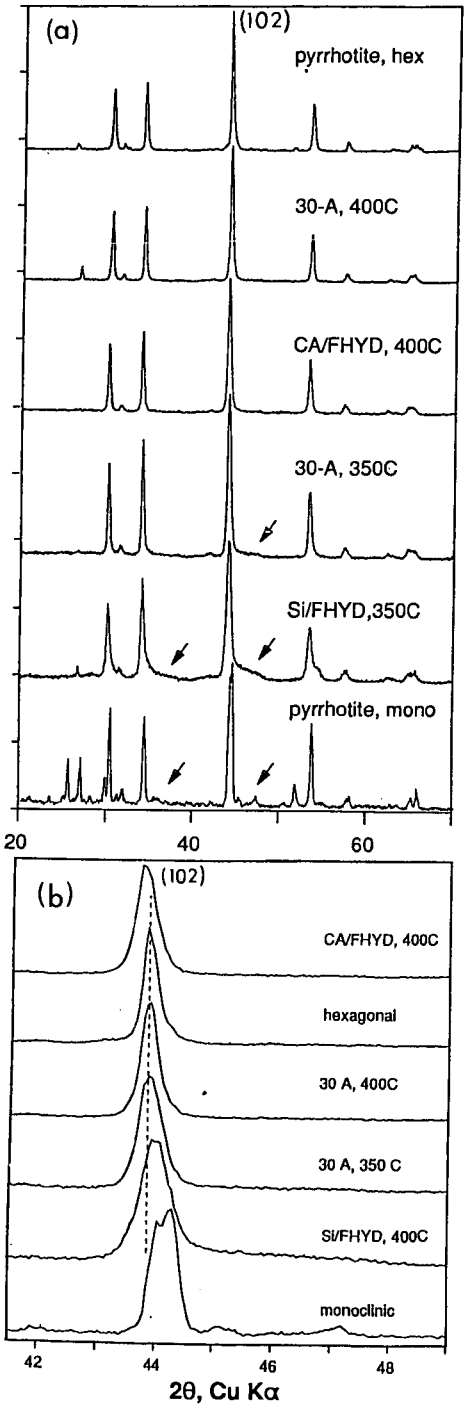

Figure 2. a) XRD patterns for the pyrrhotites and the sulfided ferrihydrite catalysts; b) the (102) peaks for the pyrrhotites and the sulfided ferrihydrite catalysts.

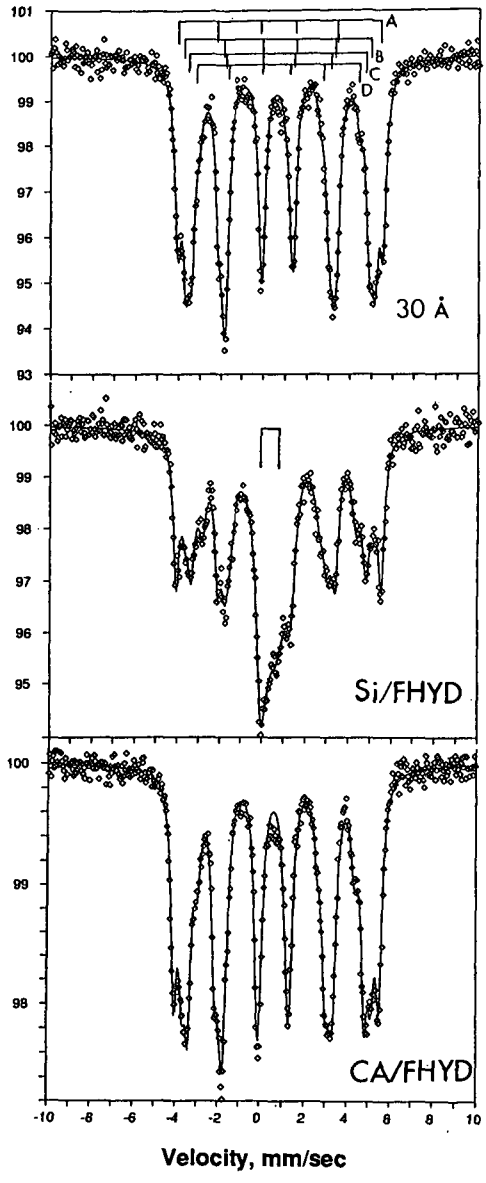

Figure 3. Mossbauer spectra of three sulfided ferrihydrites.

SOL-GEL PREPARATION OF ZIRCONIUM OXIDE

David A. Ward and Edmond I. Ko
Department of Chemical Engineering
Carnegie Mellon University
Pittsburgh, PA 15213-3890

Keywords: sol-gel preparation, aerogel, zirconium oxide (zirconia)

INTRODUCTION

A sol-gel preparation involves first the formation of a sol, which is a suspension of solid particles in a liquid, then of a gel, which is a diphasic material with a solid encapsulating a liquid. The liquid can be removed from a gel by either conventional drying (such as by using an oven) to obtain a product known as a xerogel, or by drying with supercritical extraction (often referred to as supercritical drying for short) to give an aerogel.

Preparing catalytic materials with the sol-gel method has received increasing attention in recent years because of its versatility and excellent control over a product's properties (1). In fact, there are a host of experimental variables, generally referred to as the sol-gel parameters, which can impact on the physical and chemical characteristics of a sample. To date, most studies have focused on sol-gel parameters that are important in the first step which is the formation of a gel. There has been relatively less work on the subsequent processing steps: aging, drying, and heat treatment. Because these steps are often interrelated (2), one should take a broader viewpoint and consider all of them in fine-tuning a sol-gel product.

In this paper we discuss our recent results on the sol-gel preparation of zirconia with an emphasis on three key parameters: the gel time, the starting precursor, and the drying conditions. In our view these parameters, when fully understood and explored, will put us in a better position to develop materials of desirable properties systematically. We are interested in zirconia because of its potential catalytic applications in general (3) and its effectiveness as a support for superacids in particular (4). Furthermore, the phase transformation of zirconia as a ceramic material is of great interest (5).

EXPERIMENTAL

We used two different precursors in our sol-gel preparation. In the first approach (6), zirconium n-propoxide was mixed with n-propanol and nitric acid. This solution was then mixed with another solution containing n-propanol and water and the mixture was vigorously stirred. The gel time was defined as the time required after mixing for the vortex created by the stirring to disappear completely. The resulting gel, known as an alcogel because alcohol was the solvent, was covered and allowed to age for 2 h at room temperature. The alcohol was subsequently removed either by drying in a vacuum oven to form a xerogel, denoted as X-Zr, or by supercritical drying with carbon dioxide to form an aerogel, denoted as A-Zr. The supercritical drying conditions were usually at ca. 343 K and 2.1×10^7 Pa and the resulting aerogel powder was subsequently vacuum dried. Aerogels that were supercritically dried at a higher temperature of 473 K were denoted as A-Zr-473.

In the second approach (7), three different size zirconia sols, provided by Nyacol Products, Inc., were used: 5-10, 50, and 100 nm. These sols were gelled by the addition of ammonium hydroxide to give samples 10-Zr-0.3, 50-Zr-0.3, and 100-Zr-0.3. The first number refers to the initial sol size in nm and 0.3 is the ratio of ammonium hydroxide to nitric acid (which provides the counter ion in the original sol). These gels were allowed to age for 2-3 h at room temperature and then vacuum dried.

The above vacuum drying steps were performed at 383 K and 3.4×10^3 Pa for 3 h. Finally, all the samples were calcined at 773 K for 2 h in flowing oxygen (24 l/h).

An Autosorb-1 gas sorption system (Quantachrome Corp.) was used to obtain nitrogen adsorption/desorption isotherms. Before analysis, all samples were outgassed at 473 K under vacuum for 2-3 h. Pore size distribution data were calculated with the BJH method (8). X-ray diffraction experiments were performed on a Rigaku D/Max Diffractometer with Cu-K_α radiation.

RESULTS AND DISCUSSION

Effect of Gel Time

At its simplest level, sol-gel chemistry involves the hydrolysis of a precursor (which is a metal alkoxide in our aerogel case) and the condensation of partially hydrolyzed species to form a three-dimensional gel network. The gel structure is thus sensitive to the rate of hydrolysis relative to that of condensation (9), and the two rates can be varied by, for example, adjusting the amounts of water and acid used in the preparation.

In our preparation of zirconia alcogels, we found that the gel time increases significantly when we increase the amount of nitric acid used (6). This observation can be understood in terms of an increased concentration of protonated hydroxo ligands with more acid, thus decreasing the condensation rate and increasing the gel time. The amount of water used also affects the gel time

by changing the concentration of the hydrolyzed species. Qualitatively a decrease in water content slows down the hydrolysis and condensation reactions, thus increasing the gel time. As an example of the effects of changing gel times, Figure 1 shows the variation of surface area and pore volume with gel time for zirconia aerogels calcined at 773 K for 2 h. A gel time of zero corresponds to the formation of a precipitate instead of a gel. This happens when no acid is used and a rapid condensation leads to particle growth. The resultant calcined product thus has very little surface area and pore volume. With increasing gel time, we slow down condensation to allow cross-linking to occur concurrent with particle growth. Hence the product has a large surface area and pore volume upon calcination. Under optimal conditions, we could stabilize a tetragonal zirconia that has a surface area of 134 m^2/g and a pore volume of 0.37 cm^3/g (see Table 1). However, with further lengthening of the gel time, condensation slows down to form a weakly cross-linked network. The collapse of this network during calcination leads to a decrease in surface area and pore volume. The variation of pore size distribution with gel time, as shown in Figure 2, is also consistent with this explanation.

In addition to macroscopic physical properties, gel time affects the microscopic "quality" of the material in terms of defect density. We found that zirconia aerogels prepared at different gel times exhibit different behavior with respect to their tetragonal-to-monoclinic phase transformation. Specifically, at a calcination temperature of 973 K, the ratio of tetragonal to monoclinic phase is a strong function of gel time. Samples with short gel times transform more readily into the monoclinic phase because they have higher defect densities (6). In sum, gel time is an important parameter in controlling the initial gel structure which impacts on all subsequent sol-gel processing steps.

Effect of Starting Precursor

In changing the rates of hydrolysis and condensation of metal alkoxides, one is balancing the growth of particles and the cross-linking of these particles. The particle size in a sol is thus a key parameter in controlling the initial gel structure. To probe this idea, we have used preformed zirconia sols as alternate precursors in order to study the effect of sol size independently. Table 1 summarizes the physical properties of zirconias prepared with three different starting sol sizes.

When solid spherical particles are packed together, the external surface area varies inversely with particle size. This trend is opposite to the data in Table 1, which shows that the sample made with the largest sol also has the highest surface area. This observation is due to the fact that the starting sol particles are not dense, but contain internal micropores which are the primary contributors to the surface area and pore volume of the resulting materials. In fact, we have found that all three zirconia samples have similar pore size distributions and are primarily microporous (7). Recall that zirconia aerogels are mesoporous (see Figure 2) and have pore volumes that are a factor of 3-5 higher (see Table 1).

Table 1 shows that the crystal structure of the 10-Zr-0.3 sample is the same as the zirconia aerogels. On the other hand, both the 50-Zr-0.3 and 100-Zr-0.3 samples contain monoclinic domains. This difference can be explained in terms of a bimodal size distribution in the two larger sols, which contain about half by weight particles in the indicated size and the other half in the 5-10 nm size range (7). Apparently the small particles crystallize into the tetragonal phase upon heat treatment while the large particles are in the monoclinic phase.

These results clearly demonstrate that using a different starting precursor (metal alkoxide versus preformed sols) is a simple and effective way to change the textural and structural properties of a sol-gel product. At the same time they teach us that a careful characterization of preformed sols, in particular their particle size distribution and porosity, is necessary for their applications as precursors.

Effect of Drying Conditions

The basic idea of supercritical drying is to eliminate the liquid-vapor interface in a pore in order to avoid differential capillary pressure in a gel network. Results in Table 1 show that physical properties of a zirconia aerogel (A-Zr) and xerogel (X-Zr) are indeed very different, with the latter having a much lower surface area and pore volume. Furthermore, the xerogel is primarily microporous. However, we note that we intentionally did not take great care in minimizing the capillary pressure in preparing the xerogel to illustrate the effect of drying conditions. There are many effective approaches, such as using a solvent with a low surface tension (10), in obtaining high-surface-area, low-density xerogels that are of catalytic interest.

We have found that varying the temperature while using a single drying agent, carbon dioxide, can also change the properties of a zirconia aerogel (11). We prepared two zirconia aerogels by supercritically drying them at 343 and 473 K. The two samples have similar surface areas, pore volumes, and crystal structures after calcination at 773 K for 2 h, but a more careful examination reveals interesting differences. First, the sample dried at 473 K has a pore size distribution that is shifted towards larger pores. The resulting larger average pore diameter explains why this sample has a larger pore volume but a smaller surface area than the sample dried at 343 K. Second, the sample dried at 473 K crystallizes into the tetragonal phase at a lower heat treatment temperature. Figure 3 shows that after calcination at 673 K for 2 h, the sample dried at 343 K remains X-ray amorphous whereas the one dried at 473 K shows a diffraction peak of tetragonal zirconia.

Our results highlight the fact that a gel is not static during supercritical drying. Indeed, drying should be considered as part of the aging process during which polymerization, coarsening, and phase transformation occur (2). While supercritical drying may be more effective in preserving a gel's network in comparison with evaporative drying, supercritical drying nonetheless accelerates aging because its operating temperature is above ambient. Along this line, we should expect aerogels that are prepared with different supercritical drying agents to have different properties. An example is the finding of Beghi et al. (12), who showed that anatase crystallization in titania-silica is more extensive when the sample is dried in alcohol (which has a higher critical temperature) than in carbon dioxide. Clearly, there are a lot of research opportunities in using supercritical drying conditions to vary the properties of aerogels.

SUMMARY
The sol-gel process has four key steps, gel formation, aging, drying, and heat treatment, each of which consists of a large number of tunable parameters. Furthermore, these steps are interrelated in that what happens in one step usually affects the next step. The initial gel structure will dictate the extent to which it is influenced by drying conditions, differently dried gels will have different structural evolution with heat treatment, and so on. However, it is important to view these complexities as opportunities in using the sol-gel method to prepare catalytic materials with desirable properties. In this paper we have shown the use of three specific parameters in changing the surface area, pore volume, and crystal structure of zirconia. Although these are physical and not chemical properties, results in our laboratory have shown that they have important catalytic implications. We believe more systematic studies are necessary to identify the key parameters in each sol-gel step and to understand the underlying physical and chemical processes. Extension to multi-component systems is of particular interest because of their widespread applications.

ACKNOWLEDGMENT
We thank the National Science Foundation (CTS-9200665) for supporting this work and Nyacol Products, Inc. for providing us with zirconia sols. D.A.W. thanks the Texaco Foundation for the support of a graduate fellowship.

REFERENCES
1. Cauqui, M. A. and Rodríguez-Izquierdo, J. M., J. Non-Cryst. Solids 147/148, 724 (1992).
2. Brinker, C. J. and Scherer, G. W., Sol-Gel Science: The Physics and Chemistry of Sol-Gel Processing; Academic: New York, 1990.
3. Tanabe, K., Mater. Chem. Phys. 13, 347 (1985).
4. Hino, M., Kobayashi, S. and Arata, K., J. Am. Chem. Soc. 101, 6439 (1979).
5. Srinivasan, R., Davis, B. H., Cavin, O. B. and Hubbard, C. R., J. Am. Ceram. Soc. 75, 1217 (1992).
6. Ward, D. A. and Ko, E. I., Chem. Mater. 5, 956 (1993).
7. Ward, D. A. and Ko, E. I., Langmuir, in press.
8. Barrett, E. P., Joyner, L. G. and Halenda, P. P., J. Am. Chem. Soc. 73, 373 (1951).
9. Livage, J., Henry, M. and Sanchez, C., Prog. Solid St. Chem. 18, 259 (1988).
10. Smith, D. M., Desphande, R. and Brinker, C. J., Mat. Res. Soc. Symp. 271, 567 (1992).
11. Brodsky, C. J. and Ko, E. I., J. Non-Cryst. Solids, in press.
12. Beghi, M., Chiurlo, P., Costa, L., Palladino, M. and Pirini, M. F., J. Non-Cryst. Solids 145, 175 (1992).

Table 1. Physical Properties of Zirconium Oxides after Calcination at 773 K for 2 h

Sample notation	BET surface area (m^2/g)	Pore volume (cm^3/g)	Crystal structure[a]
A-Zr[b]	134	0.37	tetragonal
A-Zr-473[c]	124	0.43	tetragonal
X-Zr	28	0.029	tetragonal
10-Zr-0.3[d]	17	0.017	tetragonal
50-Zr-0.3[d]	131	0.087	tetragonal + monoclinic
100-Zr-0.3[d]	149	0.124	tetragonal + monoclinic

[a] Determined by X-ray diffraction; [b] Taken from (6); [c] Taken from (11); [d] Taken from (7).

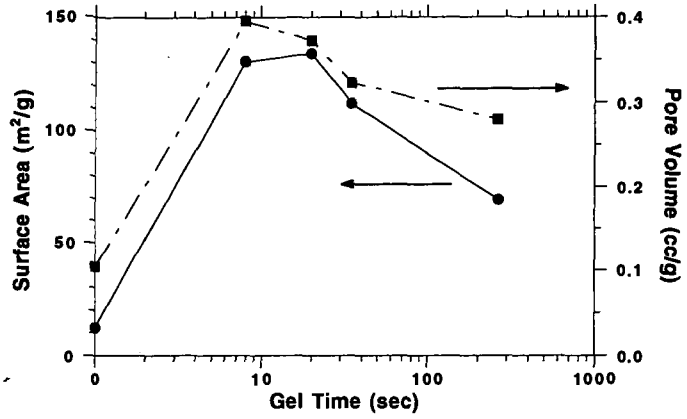

Figure 1. Effect of gel time on the physical properties of zirconia aerogels after calcination at 773 K for 2 h

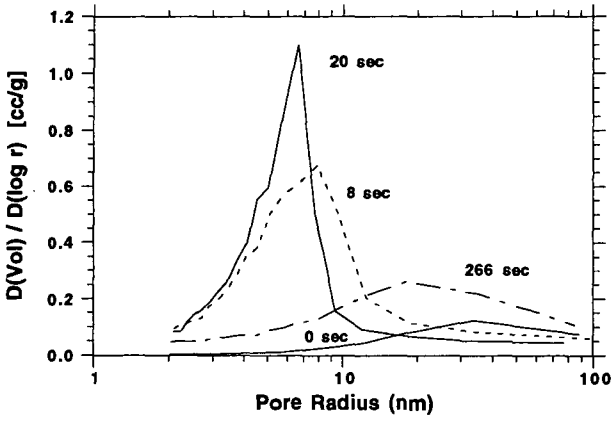

Figure 2. Effect of gel time on the pore size distribution of zirconia aerogels after calcination at 773 K for 2 h

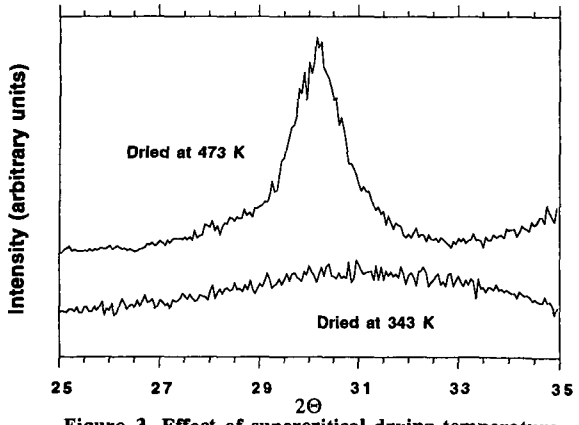

Figure 3. Effect of supercritical drying temperature on the crystallization of zirconia aerogels after calcination at 673 K for 2 h

CATALYTIC HYDRODENITROGENATION OF QUINOLINE WITH NANOSCALE Mo_2N, Mo_2C and MoS_2 SYNTHESIZED BY LASER PYROLYSIS

[1]R. Ochoa, [2]W.T. Lee, [1,2]P.C Eklund,
[1]Center for Applied Energy Research
[2]Department of Physics and Astronomy,
University of Kentucky, Lexington KY 40511.

KEYWORDS: Laser Pyrolysis, hydrodenitrogenation, molybdenum nitride, molybdenum carbide

INTRODUCTION

As the quality of available petroleum feedststocks decreases, the demand for better and more active catalysts for hydrotreatment increases. Nitrogen content in coal, tar sands, shale and petroleum residua is present predominantly in the form of heterocyclic compounds. Quinoline constitutes a molecule representative of these heterocyclic compounds and its catalytic denitrogenation is one of the most studied model compound reactions. Due to the considerable number of stable reaction intermediates with different absorptivities and reactivities, this reaction is a typical example of the complexity of the denitrogenation process.

Nitrogen removal from heterocyclic compounds is a more difficult process than sulfur removal. It has been accepted that it requires hydrogenation of the ring containing the nitrogen atom before hydrogenolysis of the carbon-nitrogen bond occurs [1,2]. This is partly due to the thermodynamics of the aliphatic C-N bond hydrogenolysis reaction.

Figure 1 shows a diagram of the reaction pathway reported by Satterfield et al [3,4] for the denitrogenation of quinoline over a sulfided $NiMo/Al_2O_3$ catalyst . It is seen that the HDN reaction proceeds through the hydrogenation of quinoline (Q) to 1,2,3,4 tetrahydroquinoline (THQ) and 5,6,7,8 tetrahydroquinoline (CHPYD), the first reaction being faster than the second. THQ can either convert into-propylaniline (O-PA), through bond cleavage of the C-N bond, or together with CHPYD, it can hydrogenate to form decahydroquinoline (DHQ) . The rapid hydrogenation of Q to THQ causes the establishment of a pseudoequilibrium among this hydrogenated derivatives of quinoline [1]. As seen in the figure, this pathway indicates that removal of nitrogen from O-PA requires the hydrogenation of the aromatic ring, consuming more hydrogen in the reaction. Therefore, it is desirable to synthesize hydrodenitrogenation catalysts that will induce nitrogen removal from the molecule without full hydrogenation of the aromatic ring.

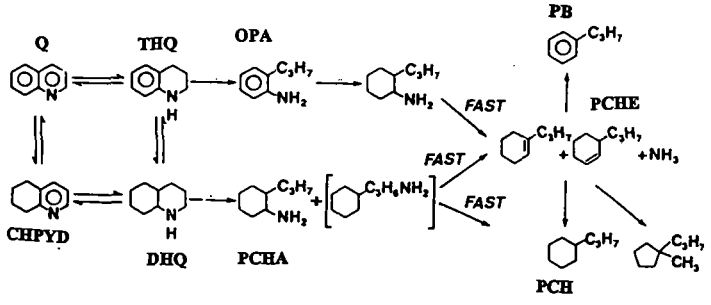

Figure 1
Reaction Pathway for quinoline HDN

It has been reported that nitrides and carbides of transition metals, specially Mo_2C and Mo_2N , synthesized by Temperature Programmed Reduction , posses high activity for heteroatom removal and hydrogenation of coal liquids and model compounds [5-7]. This work presents the results of the evaluation of the catalytic activity of Mo_2N, MoS_2 and Mo_2C ultrafine particle catalysts (UFP), synthesized by laser pyrolysis, for quinoline hydrodenitrogenation (HDN) .

EXPERIMENTAL

Mo-based ultrafine particle catalysts (Mo_2C, Mo_2N,MoS_2) were produced by laser pyrolysis from the reaction of $Mo(CO)_6$ with a gaseous reactant (NH_3, C_2H_4 or H_2S) followed by surface passivation in a flow of 5%O_2 balanced He at 300 K. The details of the experimental procedure and apparatus have been reported elsewhere [8,9].

The catalysts structure and morphology have been characterized by X-ray diffraction, high resolution-tranmission electron microscopy (HR-TEM) and thermogravimetry-mass spectrometry (TG-MS) [8-11]. The surface area was determined by the nitrogen BET method. The average composition of these particles was obtained by elemental analysis and the chemical state of the surface was characterized by X-ray photoelectron spectroscopy. Irreversible chemisorption of CO was used to measure the number of active sites on the catalyst surface.

Catalytic activity was evaluated using a stainless steel bomb microreactor, 22 cm^3 in volume, which was pressurized at 800 psi of hydrogen. A 5% catalyst loading with respect to a solution of quinoline dissolved in hexadecane was used. The reactor was maintained at 380°C for reaction periods of 15, 30 and 60 min while agitating at 440 rpm in a fluidized sand bath. The effect of the presence of added sulfur in the reaction was studied by adding dimethyl disulfide (DMDS) in 20% excess of the stoichiometric amount required to convert Mo_2N and Mo_2C to MoS_2. The liquid products were analyzed by gas chromatography with a fused-silica 30 m capillary DB5 column with a Flame Ionizing Detector. In this model compound reaction, the concentration of the liquid phase products is given as a mole percentage of quinoline initially charged to the reactor and normalized to 100%.

RESULTS AND DISCUSSION

Characterization

Table 1 summarizes the structural properties of these materials together with those from the commercial catalyst Shell 324.

TABLE 1

Catalyst	Surface area m^2/g	Crystallite size (nm)	Particle size (nm)	Site Density $x10^{15}cm^{-2}$
fcc Mo_2N	63	3	10	0.92
fcc Mo_2C	75	2	8.5	0.24
hex. MoS_2	86	2	4.3	na
Shell 324*	160	11	7.9	0.27

* From ref [12].

X-ray diffraction and HR-TEM have shown that Mo_2C and Mo_2N exhibit a face centered cubic structure whereas MoS_2 has an hexagonal structure. The crystallite size of the UFP catalysts was calculated from the full width at half maximum of the corresponding x-ray diffraction lines and the particle size from the value of the surface area of the particle using $Dp=6/\rho S$, where S is the surface area of the particle and ρ is the mass density. The difference observed between particle size and crystallite size indicates that these particles are partially agglomerated. Notice that Mo_2N posseses a density of active sites almost four times higher than that of Mo_2C. However the number of active sites measured is about half of the reported for materials synthesized by Temperature Programmed Reduction [6]. Elemental analysis gave an average composition for Mo_2N of $Mo_2N_{0.77}C_{0.5}$ and $Mo_2C_3O_{0.9}$ for the molybdenum carbide. Since this particles are so small, the high oxygen content observed in the results can be accounted for as an oxide monolayer of MoO_3 on the particle surface, as confirmed by XPS analysis [10].

Catalytic Activity

Figure 2 presents the results from the conversion of quinoline with respect to reaction time over Mo_2N, Mo_2C and MoS_2 UFP. It is observed that all three catalysts gave approximately the same high level of conversion. However, because there are numerous nitrogen-containing intermediate products, a high quinoline conversion does not necessarily correlate with high HDN conversion. In this case, quinoline was converted essentially into tetrahydroquinoline (THQ).

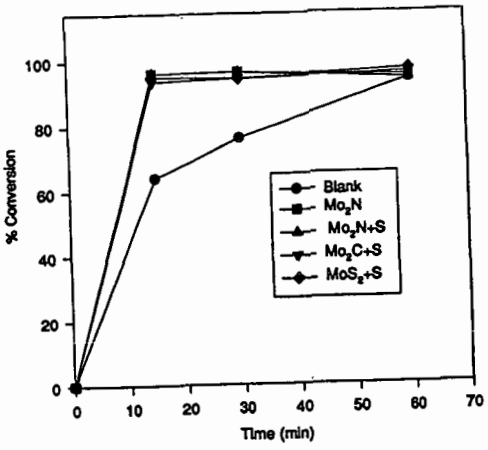

Figure 2
Conversion of quinoline with respect to time over Mo_2N, Mo_2C and MoS_2.

Figure 3 presents the product distribution for quinoline over the molybdenum nanoparticles after 30 minutes of reaction. The results are also compared to those of the commercial catalysts Shell 324 which was sulfided prior to the reaction.

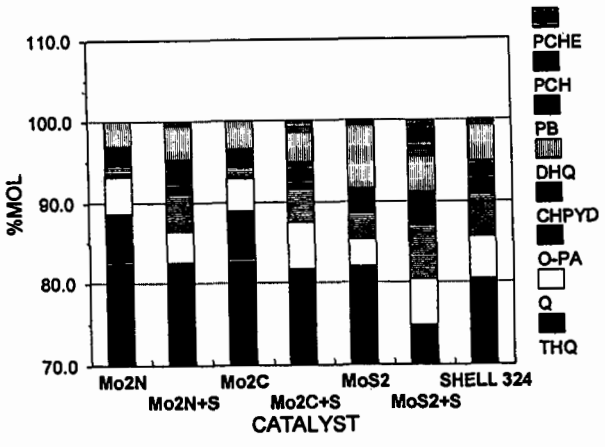

Figure 3. Product distribution after 30 minutes of reaction time

As it was previously mentioned, the main product of the reaction is THQ, in concentrations higher than 70% mol. This high concentration is thermodinamically favored by the elevated hydrogen pressure at which the reaction was carried out [1]. Mo_2C and Mo_2N gave very similar product distribution and concentration. This may be explained in terms of the similarity in surface composition observed from the xps analysis of these two catalysts [10]. Besides THQ, o-propylaniline (O-PA) , decahydroquinoline (DHQ) and cyclohexenopyridine (CHPYD) were also produced, while no denitrogenated products were detected. A higher concentration of DHQ (8%) and a small amount of propylbenzene (PB) were produced in the presence of MoS_2. Notice that Shell 324 gave similar conversion as MoS_2.

Longer reaction time periods (Figure 4) induced the conversion of tetrahydroquinoline (THQ) mainly into hydrogenated products, primarily decahydroquinoline (DHQ) with some THQ being dehydrogenated back to quinoline. Only small concentrations of nitrogen-free molecules were detected, less than a total of 1 % mol.

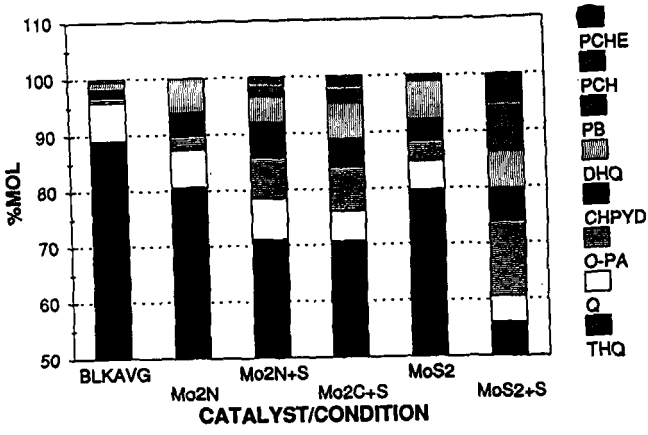

Figure 4. Product Distribution after 60 minutes of reaction time.

When excess sulfur was added to the reaction mixture, the concentration of THQ decreased, especially in the case of MoS_2, indicating that it was converted into other reaction products. Furthermore, the average concentration of hydrogenated products did not seem to be affected as much as the concentration of propylaniline (O-PA), which increased by more than 200% for the three catalysts. This fact agrees with previous reports that the presence of H_2S enhances hydrogenolysis reactions [1,2]. An increase in the concentration of denitrogenated compounds, mainly propylcyclohexane (PCH) and propylcylohexene (PCHE) was also observed. Only small concentrations of propylbenzene (PB) (~1-2%) were detected in the product mixture. This result agrees with the reaction pathway shown in figure 1. According to this figure, propylaniline (OPA) is hydrogenated to propylcyclohexylamine, which undergoes rapid denitrogenation to produce propylbenzene (PB), propylcyclohexene (PCHE) and propylbenzene (PB). In addition, decahydroquinoline (DHQ) undergoes hydrogenolysis of the C-N bond to produce propylcyclohexylamine.

Since the concentration of decahydroquinoline (DHQ) does not increase, but in some cases decreases, while the concentration of propylaniline (OPA) increases, it follows that the denitrogenation of decahydroquinoline (DHQ) is favored over the hydrogenation of O-PA. X-ray diffraction of the spent catalysts indicates that there is some transformation of Mo_2N and Mo_2C into MoS_2 after 60 minutes of reaction. This may explain why all three catalysts seem to follow the same reaction pathway.

HDN Activity

The Mo-based ultrafine particles exhibited low activity for HDN even in the presence of added sulfur. This low activity was unexpected, since there are reports of higher conversions and high selectivity for Mo2C and Mo2N catalysts, even under sulfur free conditions [6]. This outcome has been attributed in part to the presence of an oxide phase on the surface of these catalysts that may inhibit their activity [13,10].

Figure 5 presents % HDN as a function of time for the Mo-based UFP catalysts in the presence of added sulfur. As it was mentioned above, in the absence of sulfur very little denitrogenation was observed (less than 1%), even if the reaction was carried out for longer time periods or at higher temperatures (up to 2 hours, 400°C).

When H_2S was present, the denitrogenation of quinoline increased from 0.5% to 3 % for Mo_2N and to 4% for Mo_2C. Considering that Mo_2C has a lower number of active sites per unit area of catalyst, it follows that it is a more active catalyst than Mo_2N. As shown by figure 5,

MoS_2 was the most active catalyst since it gave the largest percent of denitrogenation (13%).

In terms of product selectivity, all three catalysts favored hydrogenated products over aromatic ones in the form of mixtures of propylcylohexane and propylcyclohexene.

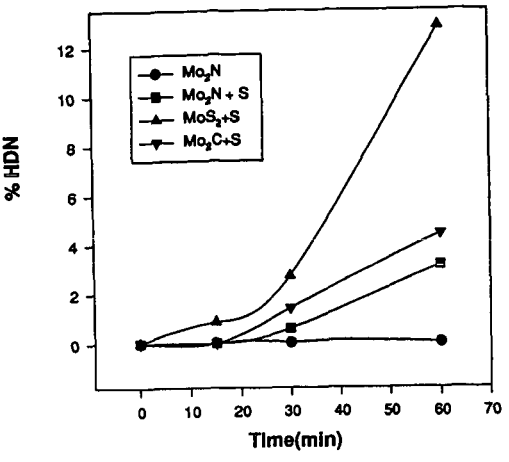

Figure 5
%HDN versus time for Mo_2N, Mo_2C and MoS_2 UFP catalysts.

CONCLUSIONS

Mo_2C, Mo_2N and MoS_2 ultrafine particle catalysts exhibited low activity and selectivity for the hydrodenitrogenation of quinoline. MoS_2 appears to be the most active catalysts . In the absence of sulfur, only less than 1% HDN was obtained with these catalysts. The addition of sulfur favored HDN activity by enhancing the hydrogenolysis of decahydroquinoline and tetrahydroquinoline. However, the improvement in activity was not very significant. The lower-than expected activity observed for this reaction, as well as for other model compound reactions tested [13], has been attributed to the presence of oxygen and amorphous carbon on the catalysts surface. In previous studies, it has been shown that surface composition has a large effect on the catalytic behavior of Mo_2C and Mo_2N specially for structure-sensitive reactions like hydrogenolysis and isomerization. Future studies to prevent or remove oxide coatings and to observe the effect on catalytic activity are underway

REFERENCES

[1] T.C. Ho, Catal. Rev. -Sci. Eng., 30(1), (1988) 117-160.

[2] M. J. Girgis, B.C. Gates, Ind. Eng. Chem. Res. 30; (1991)2021-2058.

[3] C.N. Satterfield, J.F. Cocchetto, Ind. Eng. Chem. Proc. Des. Dev. 17, (1978) 141

[4] C.N. Satterfield, S.H. Yang, Ind. Eng. Chem. Proc. Des. Dev.23, (1984) 11

[5] S.T. Oyama, R. Kapoor, C. Shudakar, Prep. of Am. Chem. Soc. Div. Fuel Chemistry, 37(1), (1992), 233.

[6] S.T. Oyama, J.C. Schlatter, J. Metcalfe, J. Lambert , Ind. Eng. Chem. Res. 27, (1988) 1648-1653.

[7] S.T. Oyama, J.C. Schlatter, J. Metcalfe, J. Lambert , Ind. Eng. Chem. Res. 27, (1988) 1639.

[8] X.X. Bi, B. Ganguly, G.P. Huffman, F.E. HUggins, M. Endo, P.C. Eklund, J. Mater. Res. 8(7), (1993) 1666.

[9] X.X. Bi, Y. Wang, W.T. Lee, K.A. Wang, S. Bandow and P.C. Eklund, Mat. Res. Soc. Symp. Proc., 327, (1994) 47-52.

[10] X.X. Bi, K.Das Chowdhury, R. Ochoa, W.T. Lee, S. Bandow, M.S. Dresselhaus and P.C. Eklund, Proc. Mat. Res. Soc. Symp T, Boston, 1994.

[11] R. Ochoa, P. Zhou, X.X. Bi, W.T. Lee, A. Rao, P.C. Eklund, ACS Prep. Div. Fuel Chem. April 1995.

[12] C. C Yu, S. Ramanathan, F. Sherif, S.T. Oyama, J. Phys. Chem., 98 (1994) 13038-13041.

[13] R. Ochoa, G.T. Hager, W.T. Lee, S. Bandow, E. Givens and P.C. Eklund, Proc. Mat. Res. Soc. Symp T, Boston, 1994.

CATALYTIC ACTIVITY OF NANOPHASE METALS PREPARED SONOCHEMICALLY

Taeghwan Hyeon, Mingming Fang, Andrzej A. Cichowlas, and Kenneth S. Suslick*

School of Chemical Sciences and Materials Research Laboratory,
University of Illinois at Urbana-Champaign, 505 S. Mathews Ave., Urbana, IL 61801
tel, 217-333-2794; fax, 217-333-2685; email, ksuslick@uiuc.edu

Keywords: ultrasound, sonochemistry, nanophase, nanostructured, heterogeneous catalysis

INTRODUCTION

The chemical effects of high intensity ultrasound arise from acoustic cavitation: the formation, growth, and implosive collapse of bubbles in a liquid, which generates a transient, localized hot spot (1, 2). The local conditions reached have temperatures of ~5000 K, pressures of ~1800 atm, but with cooling rates that exceed 10^{10} K/s (3, 4). We have made use of these extreme conditions to develop a new technique for the synthesis of nanostructured heterogeneous catalysts. When irradiated with high intensity ultrasound in low volatility solvents under argon, volatile organometallic precursors produce high surface area solids that consist of agglomerates of nanometer clusters. These nanostructured solids are active heterogeneous catalysts for hydrocarbon reforming and CO hydrogenation. For Fe and Co, nanostructured alloys can be formed of any composition. Using polymeric ligands or oxide supports, the initially formed nanoscale clusters can be trapped as colloids or supported catalysts, respectively.

A central focus of recent work in materials chemistry has been the preparation of nanostructured materials (5, 6). A variety of chemical and physical preparative methods have been applied to produce materials with nanometer structure; these include metal evaporation (7), decomposition of organometallic compounds (8), and the reduction of metal salts (9, 10). Sonochemical decomposition of transition metal carbonyl compounds has also been proven to be a useful technique to generate nanophase transition metals (11, 12).

One of the advantages of our sonochemical synthesis of nanostructured materials is that various forms of nanophase materials can be generated simply by changing the reaction medium. When precursors are sonicated in high boiling alkane such as decane or hexadecane, nanostructured powders are formed. Using a polymeric ligand (e.g. polyvinylpyrrolidone (PVP)) or inorganic support (silica, alumina, etc.), nanophase metal colloids and nanostructured supported metal catalysts are generated (Scheme 1). A transmission electron micrograph of the nanocolloid Fe/PVP is shown in Figure 1.

EXPERIMENTAL SECTION

All manipulations for the preparation of samples were performed using Schlenk vacuum line and inert atmosphere box (Vacuum Atmospheres, < 1 ppm O_2) techniques. Pentane was distilled over sodium-benzophenone. Decane and hexadecane were distilled over sodium. Ultrasonic irradiation was accomplished with a high intensity ultrasonic probe (Sonic and Materials, model VC-600, 1 cm Ti horn, 20 kHz, 100 Wcm^{-2}).

X-ray powder diffraction data were collected on a Rigaku D-max diffractometer using Cu K_α radiation (λ = 1.5418 Å). Scanning electron micrographs were taken on a Hitachi S800 electron microscope. Transmission electron micrographs were taken on a Phillips CM-12 electron microscope. Samples for elemental analysis were submitted in sealed vials without exposure to air.

Hydrogen (99.99%, Linde), methane (99.97%, Matheson) and CO (99.0+%, Linde) were further purified through 5 Å molecular sieves and oxy-traps (Alltech). Cyclohexane (99+%, Fischer) was dried over molecular sieves prior to use. In cyclohexane reaction, a MKS mass flow controller maintained the flow of hydrogen at 27.5 cm^3 (STP)/min to carry the cyclohexane vapor at a constant partial pressure of 0.1 bar through the catalyst. A quartz reactor was used for both adsorption and gas-solid catalytic studies. The catalysts were transferred from an inert atmosphere box to the catalytic rig without exposure to air. Surface areas were calculated by applying the BET equation to the N_2 adsorption isotherm measured at 77 K. The gas products obtained during the temperature-programmed desorption (TPD) and temperature-programmed reaction (TPR) experiments were analyzed by a quadruple mass spectrometer (Spectra Instruments). The catalytic reaction products were analyzed by gas chromatography (Hewlett-Packard 5730A) on a n-octane/Porasil C column with flame ionization detector.

RESULTS AND DISCUSSION

Synthesis and catalytic studies of nanostructured silica-supported Fe

Ultrasonic irradiation of decane solutions of iron pentacarbonyl, $Fe(CO)_5$, in the presence of silica gel produces a silica-supported amorphous nanostructured iron. Silica gel (Universal Scientific Incorporated chemicals, 63-100 mesh) was pretreated at 450°C under vacuum ($1x10^{-5}$ Torr) for 10 hours before use. A solution of $Fe(CO)_5$ in dry decane was added to this, and the slurry was irradiated at 20°C with a high-intensity ultrasonic probe for 3 hours under argon. After irradiation, the black powder was filtered and washed with dry pentane in an inert atmosphere box. The iron loading on silica can be easily varied by

changing the initial concentration of the $Fe(CO)_5$ solution. Elemental analysis reveals Fe, Si, O and a trace amount of carbon (<1%) to be present. The origin of carbon most likely arises from the decomposition of CO or the alkane solvent during ultrasonic irradiation. Conventional silica-supported crystalline iron catalysts were prepared using the incipient wetness impregnation method by dissolving $Fe(NO_3)_3 \cdot 9H_2O$ in an aqueous solution containing silica gel. These samples were dried at 220°C for 12 hours, and calcined at 450°C under an O_2 flow for 1 hour. Reduction of iron supported on silica was carried out in a flow of hydrogen for 1 hour at 200°C, for 1 hour at 300°C, and finally for two hours at 450°C.

Transmission electron microscopy shows that the iron particles produced by sonolysis of $Fe(CO)_5$ were highly dispersed on the silica surface. The iron particles range in size from 3 to 8 nm. Chemisorption of CO allowed measurement of the dispersion and the average particle size of the iron supported on the silica surface (13). CO chemisorption measurement data at -78°C show the average iron particle size to be ≈7.3 nm, which corresponds well with TEM data.

The catalytic activity of the silica supported nanostructured iron was probed in the commercially important Fischer-Tropsch synthesis reaction (i.e., hydrogenation of CO). Figure 2 compares the activity (in terms of turnover frequency of CO molecules converted per catalytic site per second) of silica-supported nanophase iron and conventional silica-supported iron (prepared by the incipient wetness method) as a function of temperature. These catalytic data were obtained at high iron loading and low dispersion to minimize the effects of support and dispersion. The sonochemically produced iron on silica catalyst is an order of magnitude more active than the conventional supported iron. Moreover, the silica-supported nanostructured iron catalyst exhibits high activity at low temperatures (<250°C) ,whereas the silica supported conventional iron catalyst has no activity. We suggest that the dramatic difference in activity between the two samples below 300°C may be due to the amorphous nature of iron and the inherently highly-defected surface formed during sonolysis of $Fe(CO)_5$ when the amorphous state of iron is preserved. Above that temperature the activity of our sonochemically prepared catalyst declines, which may be due to crystallization, surface annealing, and deactivation of the catalyst as result of surface carbon deposition.

Differences between the catalytic properties of the nanostructured iron and of conventional supported catalysts are also observed in selectivities of hydrocarbon synthesis. Under our conditions, the major reaction products for both catalysts are short chain C_1-C_4 hydrocarbons and CO_2. Product distribution of hydrocarbons showed that at temperatures lower than 275°C, the silica-supported nanostructured iron catalyst shows higher selectivity towards long chain hydrocarbons (C_{5+}), whereas the conventional supported iron shows no activity at these temperatures. At temperatures higher than 275°C, the reaction product distributions are similar for both types of catalysts.

Synthesis and catalytic studies of nanostructured Fe-Co alloys

$Fe(CO)_5$ and $Co(CO)_3(NO)$ were chosen as precursors because of their high vapor pressures at modest bulk solution temperatures where they are still thermally stable. Solutions of $Fe(CO)_5$ and $Co(CO)_3(NO)$ at various relative concentrations in dry decane were irradiated at 0°C with a high-intensity ultrasonic probe for 3 hours under argon. After irradiation, a black powder was formed, which was filtered and washed with dry pentane in the glove box. The composition of the Fe-Co alloys can be controlled simply by changing the ratio of solution concentrations of the precursors; any alloy compositions ranging from pure Fe to pure Co can be readily obtained.

The solid-solution nature of the alloys was confirmed by TEM-EDX results, which were made on different spots of the polycrystalline alloy powders. The EDX results show that the alloys are homogeneous on a nanometer scale. The original Fe, Co, and Fe-Co alloys produced by ultrasound are porous, coral-like agglomerates of few-nanometer sized clusters; they are structurally amorphous on the nm scale, as determined by XRD, electron-beam microdiffraction, and DSC. After heat treatment under H_2 gas flow at 400°C for 2 hours, all samples underwent an irreversible crystallization, as shown by both DSC and XRD. The XRD results show no peaks attributable to iron/cobalt oxide, iron/cobalt carbide or other iron/cobalt impurity phases. Pure Fe crystallizes to cubic (bcc) structure, pure Co crystallizes to cubic (fcc) and hexagonal (hcp) mixed structures. All the alloys that we have tested so far crystallize in the bcc structure, which is consistent with the known Fe-Co equilibrium phase diagram (14). Elemental analysis results show that nearly pure metal and alloys are produced. SEM at high magnification indicates that these materials are porous aggregates of small clusters of 10-20 nm particles. Surface electronic structures and surface compositions of the sonochemically prepared Fe-Co alloys were also examined by using x-ray photoelectron spectroscopy (XPS). The XPS measurements have been performed on heat treated samples before catalytic reactions. The electronic structures of the surfaces of these samples appear to be the same as the pure metals. The surface compositions of the alloys demonstrate some small enrichment of Fe over Co. Similar trends towards an iron-enriched surface have been reported by other researchers with other preparations using coprecipitation methods (15).

Catalytic studies of the sonochemically prepared Fe-Co alloys were made on the reactions of cyclohexane: i.e., dehydrogenation versus hydrogenolysis. These reactions provide a useful pair of structure sensitive catalytic reactions to probe the nature of the sonochemically prepared nanophase catalysts. All catalysts were treated under H_2 gas flow at 400°C for 2 hours before the catalytic studies. The catalytic activity (in terms of turnover frequency of cyclohexane molecules converted to benzene per surface Fe/Co atom per second) as a function of temperature is shown in Figure 3. Two kinds of products were formed during the

cyclohexane reaction: benzene was the only dehydrogenation reaction product and aliphatic hydrocarbons (mostly methane) were the hydrogenolysis reaction products. The catalytic selectivity (in terms of the percentage of benzene among all the reaction products) as a function of temperature is shown in Figure 4. The catalytic properties of the sonochemically prepared Fe, Co and Fe-Co alloys in the cyclohexane reaction exhibit interesting trends. First, they are all active catalysts for cyclohexane conversion: pure Co has the highest activity (albeit primarily for hydrogenolysis), pure Fe has the lowest activity, and Fe-Co alloys have intermediate activity between pure Fe and pure Co. Second, Fe-Co alloys generate much more dehydrogenation product (benzene) than pure Fe or Co. Third, the 1:1 Fe/Co alloy has both much higher dehydrogenation activities and selectivities at all reaction temperatures (250°C to 300°C) than the other alloys or pure metals. In the best cases, the selectivity for dehydrogenation approaches 100%. The origin of this dramatically improved selectivity is under further investigation.

CONCLUSIONS

Sonochemical decomposition of volatile organometallic precursors in high boiling solvents produces nanostructured materials in various forms with high catalytic activities. Sonication of iron pentacarbonyl with silica in decane at 20°C generated supported amorphous nanostructured Fe on silica catalyst. The nanostructured Fe on silica catalyst showed higher catalytic activity for the Fischer-Tropsch synthesis compared to the conventional Fe/silica catalyst prepared by incipient wetness method. Sonochemical decomposition of $Fe(CO)_5$ and $Co(CO)_3(NO)$ in decane at 0°C generated nanostructured Fe and Co metals and Fe-Co alloys. The sonochemically prepared Fe-Co alloys have large surface areas relative to bulk metal even after heat treatment. We find very high catalytic activity for these Fe, Co, and Fe-Co powders for the dehydrogenation and hydrogenolysis of cyclohexane. The sonochemically prepared Fe-Co alloys show high catalytic activity for the dehydrogenation of cyclohexane to benzene, with 1:1 ratio Fe-Co alloys having selectivities as high as 100%.

ACKNOWLEDGMENTS

This work was supported by National Science Foundation. We thank Peggy Mochel, Vania Petrova, and the UIUC Center for Microanalysis of Materials, supported by the US Department of Energy, for their assistance in the electron microscopic studies.

REFERENCES

1. K.S. Suslick, *Science 247*, 1439 (1990).
2. K.S. Suslick, in K.S. Suslick (eds.), *Ultrasound: Its Chemical, Physical, and Biological Effects*, VCH Press, New York, 1988, p. 123.
3. E.B. Flint and K.S. Suslick, *Science 253*, 1397 (1991).
4. K.S. Suslick, R.E. Cline and D.A. Hammerton, *J. Amer. Chem. Soc. 106*, 5641 (1986).
5. H. Weller, *Adv. Mater. 5*, 88 (1993).
6. G.A. Ozin, *Adv. Mater. 4*, 612 (1992).
7. S.C. Davis and K.J. Klabunde, *Chem. Rev. 82*, 152 (1982).
8. A.S. Lisitsyn, A.V. Golovin, A.L. Chuvilin, V.L. Kuznetsov, A.V. Romanenko, A.F. Danilyuk and Y.I. Yermakov, *Appl. Catal. 55*, 235 (1989).
9. H. Boennemann, W. Brijoux R. Brinkmann and T. Joussen, *Angew. Chem., Intl. Ed. Engl. 129*, 273 (1990).
10. K.-L. Tsai, J.L. Dye, *J. Amer. Chem. Soc. 113*, 1650 (1991).
11. K.S. Suslick, S.B. Choe, A.A. Cichowlas and M.W. Grinstaff, *Nature 353*, 414 (1991).
12. M.W. Grinstaff, M.B. Salamon and K.S. Suslick, *Phys. Rev. B 48*, 269 (1993).
13. Dumesic, J. A.; Topsφe, H.; Boudart, M. *J. Catal. 37*, 513 (1975).
14. T. Nishizawa and K. Ishida, *Bull. Alloy Phase Diagrams 5*, 250 (1984).
15. M. Nakamura, B. J. Wood, P. Y. Hou, and H. Wise in *Proc. 4th Intl. Congr. Catal., Tokyo,* Kodansha Ltd., Tokyo, 1981, p. 432.

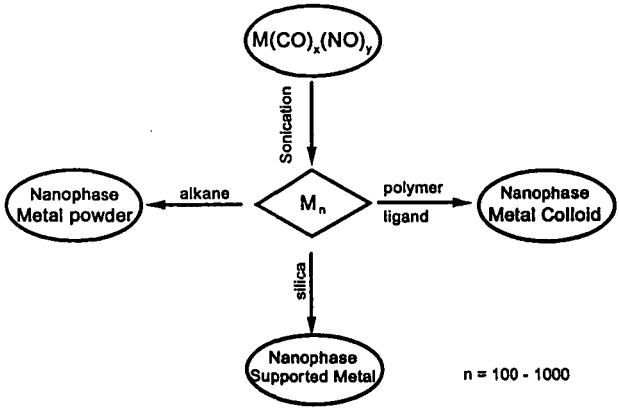

Scheme 1. **Sonochemical synthesis of various forms of nanostructured materials.**

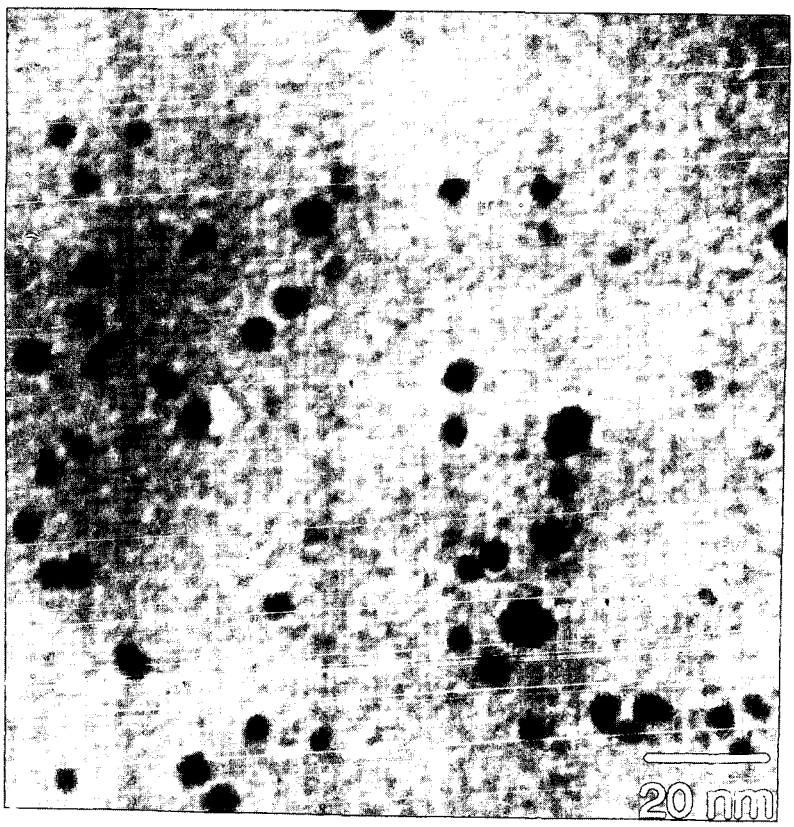

Figure 1. **Transmission electron micrograph of nanostructured Fe/PVP, obtained on a Phillips 420 electron microscope.**

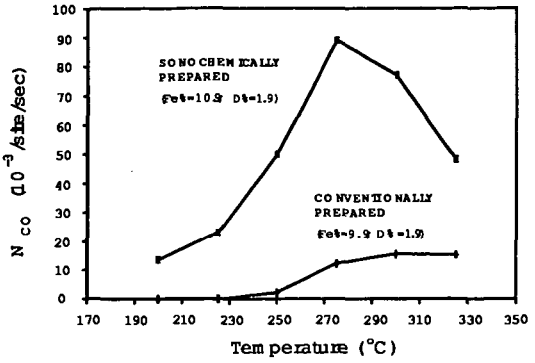

Figure 2. The catalytic activity for Fischer-Tropsch synthesis as a function of temperature. Silica-supported nanostructured iron catalyst prepared by ultrasonic irradiation of a decane solution of $Fe(CO)_5$ slurried with silica (iron loading wt% = 10.94, and dispersion, D% = 1.85) compared to conventional silica-supported crystalline iron catalyst prepared by the incipient wetness method (Fe wt% = 9.91, D% = 1.86). $H_2/CO = 3.48$, 1 atm.

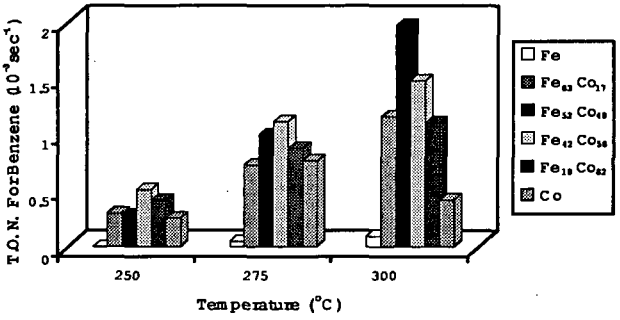

Figure 3. The catalytic activity of Fe, Co, and Fe-Co alloys for dehydrogenation of cyclohexane to benzene as a function of temperature.

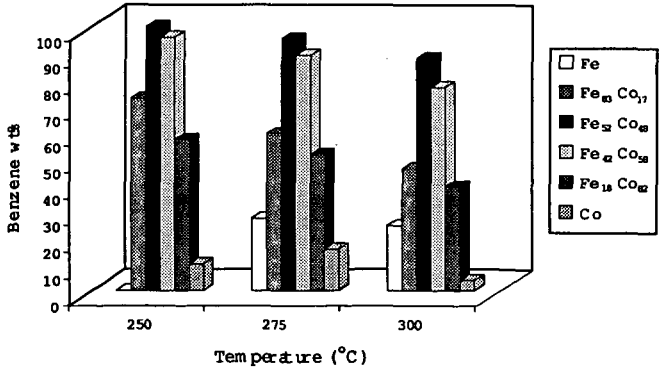

Figure 4. The catalytic selectivity of Fe, Co, and Fe-Co alloys for dehydrogenation versus hydrogenolysis of cyclohexane as a function of temperature.

THE EFFECT OF CATALYST DISPERSION ON THE ACTIVITY OF UNSUPPORTED MOLYBDENUM CATALYSTS

Anthony V. Cugini, Donald V. Martello, Donald Krastman, John P. Baltrus, Michael V. Ciocco, Elizabeth F. Frommell, and Gerald D. Holder*

U.S. Department of Energy/PETC, P. O. Box 10940, Pittsburgh, PA, 15236 (*University of Pittsburgh, Department of Chemical and Petroleum Engineering)

INTRODUCTION

Unsupported catalysts have received considerable attention for coal liquefaction. These catalysts have been introduced into coal liquefaction systems by impregnation of the coal, as water-soluble salts, as volatile metal carbonyls, as oil-soluble organometallics, as finely divided powders, and as mineral matter associated with the coal and/or solvent.[1] For the most part, the method of catalyst precursor addition affected the observed catalyst performance. Weller et al.[2] found that, with ammonium heptamolybdate, coal impregnation resulted in higher coal conversions than physical mixing of the powder with coal. Others[3,4] have also observed this result. Additionally, Derbyshire et al.[4] found that the conditions used to dry the impregnated coal (removing the aqueous solvent used for solubilizing the catalyst precursor) affected the activity of the molybdenum. Joseph[5] and Artok et al.[6] reported that expanding the coal structure (by swelling during impregnation) improved the observed activity of the catalyst, possibly by allowing better contacting of the coal with the catalyst. Schlesinger et al.[7] found that results approaching those of impregnated MoS_2 could be obtained by thoroughly mixing a powdered catalyst with the coal using a ball-mill.

The results from the study of Schlesinger et al. suggests that it is difficult to determine if the mode of catalyst addition is important because of enhanced coal/catalyst contacting or if the mode of addition affects catalyst dispersion (i.e. the physical properties, surface area and/or particle size) of the ultimate catalyst. Other studies[8-11] have shown the importance of catalyst dispersion in determining the activity of unsupported molybdenum catalysts. Related work[12] demonstrated the importance of catalyst dispersion on iron catalyst activity.

The objective of this study was to decouple the coal/catalyst contacting and catalyst dispersion and to quantify the importance of both variables.

EXPERIMENTAL

Feedstocks: The coals selected for use in this study had similar composition, but quite different particle sizes. Analyses of these coals, DECS-6 and DECS-17 Blind Canyon bituminous coals from the Department of Energy Coal Sample Base at Pennsylvania State University, are summarized in Table 1. Ammonium heptamolybdate (AHM), MoS_2, ferric nitrate, and elemental sulfur were obtained from Fisher Chemical Co., tetrahydrofuran (THF), and ammonium tetrathiomolybdate (ATTM) from Aldrich Chemical Co. PANASOL®, a mixture of alkylated naphthalenes, was obtained from Crowley Chemical Co.

Coal Impregnation: Coal was impregnated with aqueous AHM using an incipient wetness technique. In the present study, 10 g of coal was wetted with an aqueous solution containing 6% by weight of molybdenum as AHM. After standing for 0.5 h, the water was removed from the wetted coal by vacuum drying at 40°C to a constant (10g) weight of coal. In some experiments where the coal was swelled during impregnation, the amount of solution necessary for incipient wetness was augmented by THF in the ratio of 9:1 THF to solution. The coal/catalyst solution/THF mixture was left to stand overnight and vacuum dried to remove the water and THF.

Catalyst Penetration and Dispersion Measurements: When coal is impregnated with a catalyst precursor, the precursor penetrates each coal particle to a limited extent. The depth of penetration into the coal particle was measured by two methods; X-ray photoelectron spectroscopy (XPS) and energy dispersive spectroscopy/scanning electron microscopy (EDS/SEM). A model LHS-10, Leybold XPS was used to determine the concentration of Mo on the surface of impregnated coal particles. The penetration of coal by the precursor was estimated by comparing the surface concentration with the overall Mo concentration impregnated into the coal. Measurements of the Mo penetration into the coal particles were made using an ETEC Autoscan Model U-1 SEM. The X-ray maps obtained from the SEM had an analytical spatial resolution on the order of 1 μm^3. These measurements were a direct check of the Mo penetration obtained from the XPS examinations.

Catalyst dispersion was characterized by transmission electron microscopy (TEM), SEM,

X-ray diffraction (XRD), and BET surface area. A JEOL 200CX TEM was used to obtain images of MoS_2 crystallites. Similarly, SEM was used to obtain catalyst images and X-ray maps of a larger size range than those obtained by TEM. XRD analysis of the MoS_2 was performed using a Rigaku computer-controlled diffractometer to estimate MoS_2 crystallite size. The XRD size estimate was confirmed by TEM examinations of the same material. BET surface area was measured using a Coulter OMNISORB 100 CX. Nitrogen adsorption was used for these measurements.

Liquefaction Studies: Experiments were conducted by adding 3.3 g of coal or impregnated coal to the 40-mL tubular microautoclave reactor with 6.6 g of PANASOL®. In experiments in which catalysts were used, 1000 ppm of Mo was added. The reactor was charged with the desired pressure of hydrogen and sealed. The pressurized reactor was then heated, either rapidly, 1-2 minutes, or slowly, 40 minutes, to the liquefaction temperature (425°C) in a fluidized sandbath. The liquefaction conditions were 425°C, 1000 psig H_2 (cold), added sulfur, and 0.5 h. Following the liquefaction period (0.5 h), the reactor was cooled and depressurized. Coal conversion was calculated from the solubility of the coal-derived products in tetrahydrofuran (THF) and in heptane as determined by a pressure filtration technique.[13]

Catalyst Preparation: Batches of powdered MoS_2, for addition as a dispersed catalyst, were prepared in microautoclaves and 1-L autoclaves. The conditions used in these preparations were similar to the conditions used in the liquefaction studies. In the microautoclave, the precursor, aqueous AHM, powdered AHM, aqueous ATTM, or powdered MoS_3, were added with PANASOL®. The conditions were 425°C, 1000 psig H_2 (cold), added sulfur, and 0.5 h (both slow and rapid heat-up of the reactor were tested). In the 1-L flow-through reactor the conditions used were 400 g PANASOL®, 10000 ppm Mo (based on PANASOL®) as aqueous AHM (12% by weight) or aqueous ATTM (3% by weight), 2,500 psig, 4 SCFH of H_2/3%H_2S, 400°C, and 0.5 h. In all cases the catalyst was recovered as the solids from a THF extraction of the reaction products.

RESULTS:

Catalyst Dispersion: MoS_2 samples were prepared with different average particle and/or crystallite sizes and surface areas. The size and surface area were varied by using different precursor types, heat-up rates, and reactor types. The XRD-determined crystallite size and surface area for the different MoS_2 preparations are shown in Table 2. Introduction of the precursors as aqueous solutions appeared to give higher levels of dispersion than the powdered precursors. The 1-L stirred autoclave resulted in significantly higher dispersion than the shaken microautoclaves and aqueous AHM in the 1-L autoclave resulted in higher MoS_2 dispersion than aqueous ATTM (by BET surface area but not by XRD). The catalyst powder produced in the 1-L autoclave had an elemental composition of 50 wt% C and 50 wt% MoS_2. SEM and TEM analysis qualitatively confirmed the relative levels of dispersion determined by BET and XRD. TEM examination of the MoS_2 produced from AHM and ATTM in the 1-L autoclave provided some explanation for the discrepancy in surface area and XRD crystallite size for the two catalysts. For the MoS_2 from AHM, the TEM analysis indicated that the particles were less than 25 Å (single layers) and were poorly crystalline. For the MoS_2 from ATTM, the TEM analysis indicated that the particles were small (perhaps less than 25 Å) but there appeared to be a longer range structure of the carbonaceous material associated with the MoS_2 that may have accounted for the lower surface area.

Liquefaction tests were made using the various MoS_2 samples with different levels of dispersion. The results are shown in Figure 1. The 0 m^2/g surface area cases in Figure 1 represent data for no catalyst added. It appears that there is a linear relationship between catalyst surface area and conversion to THF and heptane soluble products. A similar trend was observed in plotting coal conversion with respect to inverse crystallite size (Figure 2). For the high surface area MoS_2, the inverse crystallite size was calculated based on single layer MoS_2 with a stack height of 6 Å. These results indicate that at a constant level of addition of MoS_2, the physical properties of the MoS_2 were very important in determining the ultimate activity observed. Note that for the one case of MoS_2 from ATTM in the 1-L autoclave, the activity was higher than predicted on the basis of surface area and lower than predicted on the basis of inverse crystallite size.

Coal/Catalyst Contacting: The DECS-6 and DECS-17 Blind Canyon coal were physically mixed with MoS_2, impregnated with AHM by incipient wetness, or impregnated with AHM by incipient wetness with swelling (using THF) during impregnation. The effect of the method of catalyst addition on liquefaction activity is shown in Figure 3. The selection of powdered MoS_2 for the physically mixed comparison was made based on evaluation of the dispersion of MoS_2

resulting from impregnation. The XRD analysis of MoS_2 resulting from impregnated AHM treated at liquefaction conditions indicates a crystallite size of 46 Å thickness to 103 Å width (46/103Å). Swelling had little effect on this size (47/90Å). The physically mixed MoS_2 powder used for comparison had a crystallite size of 25/77Å. The results presented in Figure 3 indicate that the method of catalyst addition influences the ultimate observed activity. One explanation for the enhancement in activity observed with the impregnation techniques is that these techniques result in penetration of the coal particle by the catalyst precursor. The penetration depths of catalyst into the coal for these cases along with the physically mixed cases are shown in Table 3. Also shown in Table 3 is the fractional volume of coal that is also occupied by the catalyst (calculated from the penetration depth). It is apparent from this table that impregnation results in enhanced penetration of the coal particle by the catalyst. EDS/SEM analyses of these sampies directly confirmed the relative penetration depths calculated from XPS data. Figures 4 and 5 present coal conversion as a function of penetration depth and fractional volume of coal occupied by the catalyst. The results indicate that the coal conversion is not so much a function of the penetration depth as it is a function of the fractional volume of coal occupied by catalyst, essentially a function of the extent of contacting between coal and catalyst. However the most significant difference in activity occurred between physical mixing and impregnation. Subtle differences (at most) were observed between the two modes of impregnation.

CONCLUSIONS:

The results of this study indicate that for catalysts with similar properties (size and surface area), the mode of catalyst addition affected the observed performance. Better catalyst performance was observed with impregnation than physical mixing. Also, for similar modes of catalyst addition, increasing the catalyst dispersion by decreasing the catalyst particle size (or increasing the surface area) results in higher observed activity. The results suggest that any comparison of catalysts should account for differences in catalyst dispersion and the mode of catalyst addition.

DISCLAIMER:

Reference in this manuscript to any specific commercial product, process, or service is to facilitate understanding and does not necessarily imply its endorsement or favoring by the United States Department of Energy.

REFERENCES:

1. Derbyshire, F.J., Catalysis in Coal Liquefaction: New Directions for Research IEA CR/08 London, UK: IEA Coal Research, June 1988.
2. Chien, P.L., Chao, H., and Weller, S.W., Ind. Eng. Chem. Proc. Des. Dev., **22**, pp 660-662 (1983).
3. Weller, S.W., Proceedings: Fourth International Conference on the Chemistry and Uses of Molybdenum, H.E. Barry and C.N. Mitchell, Ed., pp 179-186 (1989).
4. Derbyshire, F.J., Davis, A., Lin , R., Stansberry, P.G., and Terrer, M.T., Fuel Processing Technology, **12**, pp 127-141(1986).
5. Joseph, J., Fuel, **70**, pp 459-464 (1991).
6. Artok, L., Davis, A., Mitchell, G.D., and Schobert, H.H., Fuel, **71**, pp 981-991 (1992).
7. Schlesinger, M.D., Frank, L.V., and Hiteshue, R.W., Bureau of Mines Report No. 6021 (1961).
8. Frety, R., Breyesse, M., Lacroix, M., and Vrinat, M., Bull. Soc. Chim. Bulg., **93**(8,9), pp 663-672 (1984).
9. Busetto, L., Ianibello, A., Pincolini, F., and Trifiro, F., Bull. Soc. Chim. Bulg. Proc. Des. Dev., **90**(12), pp 1233-1248 (1981).
10. Ratnasamy, P. and Leonard, A.J., Journal of Catalysis, **26**, pp 352-358 (1972).
11. Utz, B.R., Cugini, A.V., and Frommell, E.A., Novel Materials in Heterogeneous Catalysis, Baker, R.T., and Murrell, L.L., Ed., ACS Symposium Series No. 437 Chapter 27 (1989).
12. Cugini, A.V., Krastman, D., Martello, D.V., Frommell, E.F., Wells, A.W., and Holder, G.D., Energy & Fuels, **8**(1), pp 83-87 (1994).
13. Utz, B.R., Narain, N.K., Appell, H.R., and Blaustein, B.D., Coal and Coal Products: Analytical Characterization Techniques, Fuller, Jr., E.L., Ed. ACS Symposium Series No. 205, p. 225 (1982).

Table 1. Analyses of Feed Coals

	Blind Canyon, DECS-6	Blind Canyon, DECS-17
Proximate Analysis, wt% as received		
Moisture	4.73	3.7
Volatile Matter	42.4	45.0
Fixed Carbon	47.3	44.9
Ash	5.6	6.3
Ultimate Analysis, wt% moisture free		
Carbon	76.5	76.2
Hydrogen	5.9	5.8
Nitrogen	1.5	1.3
Sulfur	0.4	0.4
Oxygen (Diff.)	9.9	9.6
Ash	5.8	6.8
Sulfur Forms, wt%		
Sulfate	0.01	0.01
Pyritic	0.02	0.02
Organic	0.37	0.41
Average Particle Size, um	397	84

Table 2. MoS_2 Pbysical Properties

Precursor	Gas, Heat-up	Reactor Type	BET Surface Area, m^2/g	XRD Crystallite Size, Å Height/Widtb
MoS_2	na	na	2.7	very ordered
AHM, Powdered	H_2/H_2S slow	Microautoclave	na	very ordered
ATTM	H_2 fast	Microautoclave	79.5	26 / 78
ATTM	N_2 fast	Microautoclave	84.4	27 / 78
ATTM	H_2 slow	Microautoclave	74.9	30 / 81
MoS_3	H_2 fast	Microautoclave	104.8	25 / 77
AHM (aq)	H_2/H_2S slow	Microautoclave	na	46 / 103
AHM (aq)	H_2/H_2S slow	1-L Autoclave	262.0	--* / 25
AHM (aq)	H_2/H_2S slow	1-L Autoclave	243.0	--* / 25
ATTM (aq)	H_2/H_2S slow	1-L Autoclave	45.0	-- */ 25

* 001 line was not observed.

Table 3. Effect of Mode of Addition and Coal Particle Size on Penetration Depth and Percent of Coal Contacted.

Particle Size, um	Mode of Addition	Penetration Depth, um	Percent of Coal Contacted, %
397	Physically Mixed	1	1.5
84	Physically Mixed	1	7.0
84	Aqueous Impregnation	4.7	29.7
397	Aqueous Impregnation	9.4	13.6
84	THF-Assisted Aqueous Impregnation	13.7	69.5
397	THF-Assisted Aqueous Impregnation	16.0	22.3

Figure 1. Effect of MoS_2 Surface Area on Blind Canyon Coal Conversion

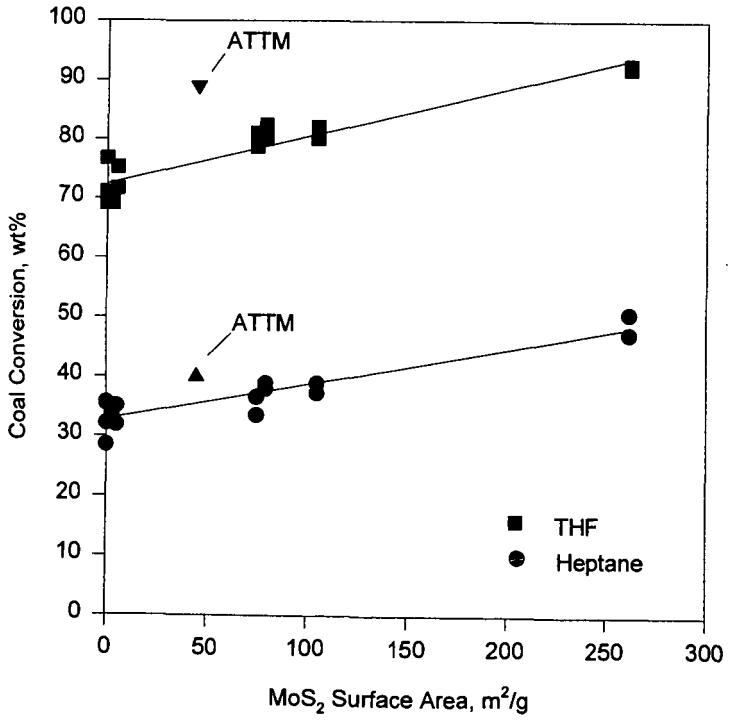

2:1 PANASOL to Coal, 425°C, 1000 ppm Mo, 1000 psig H_2 (cold) and 0.5 h

Figure 2. Effect of MoS_2 Inverse Crystallite Size on Blind Canyon Coal Conversion

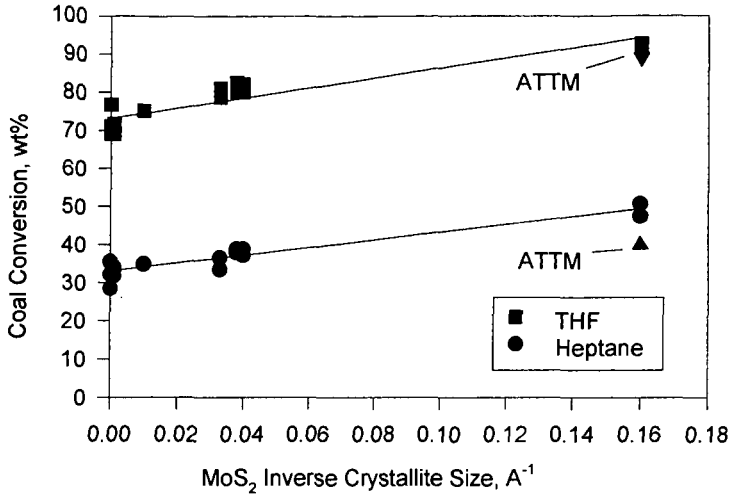

2:1 PANASOL to Coal, 425°C, 1000 ppm Mo, 1000 psig H_2 (cold), and 0.5 h

Figure 3. Effect of Method of Catalyst Addition

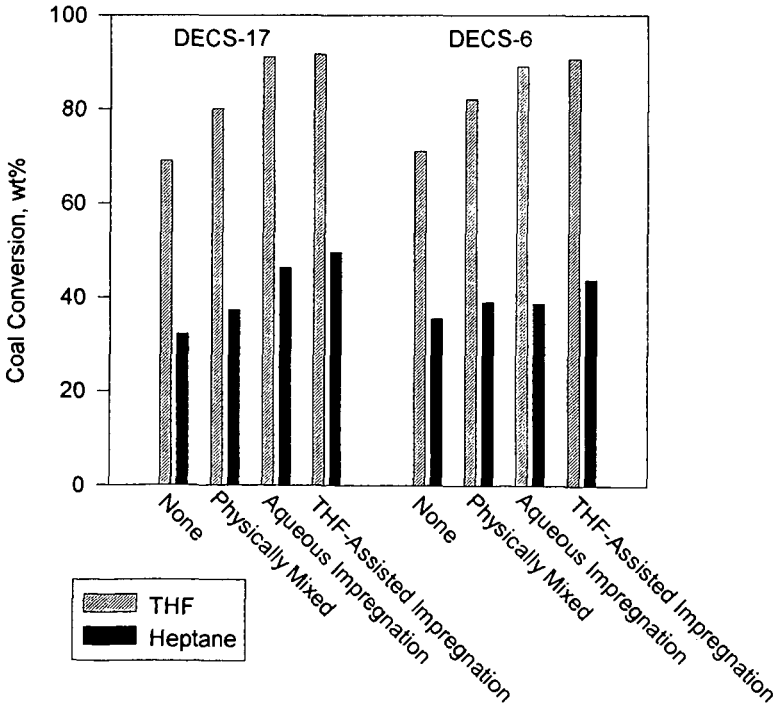

2:1 PANASOL to Coal, 425°C, 1000 ppm Mo, 1000 psig H_2 (cold), and 0.5 h

Figure 4. Effect of Penetration Depth on Blind Canyon Coal Conversion

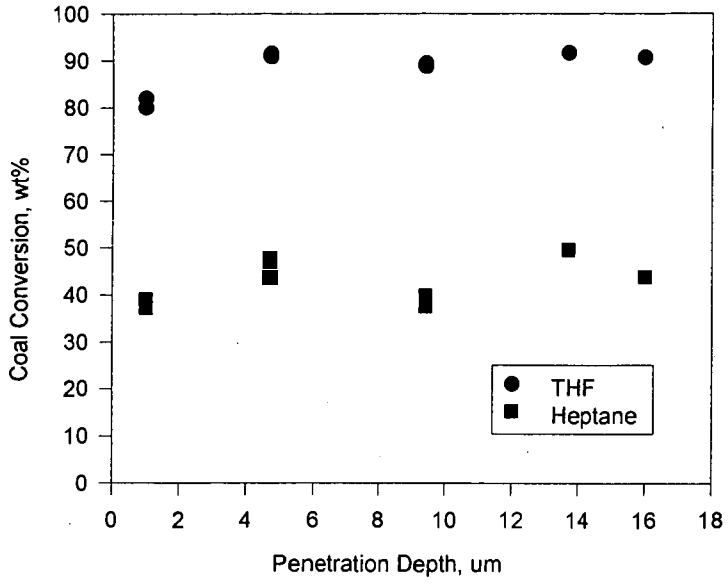

2:1 PANASOL to Coal, 425°C, 1000 ppm Mo, 1000 psig H_2 (cold), and 0.5 h

Figure 5. Effect of Coal Contacted on Blind Canyon Coal Conversion

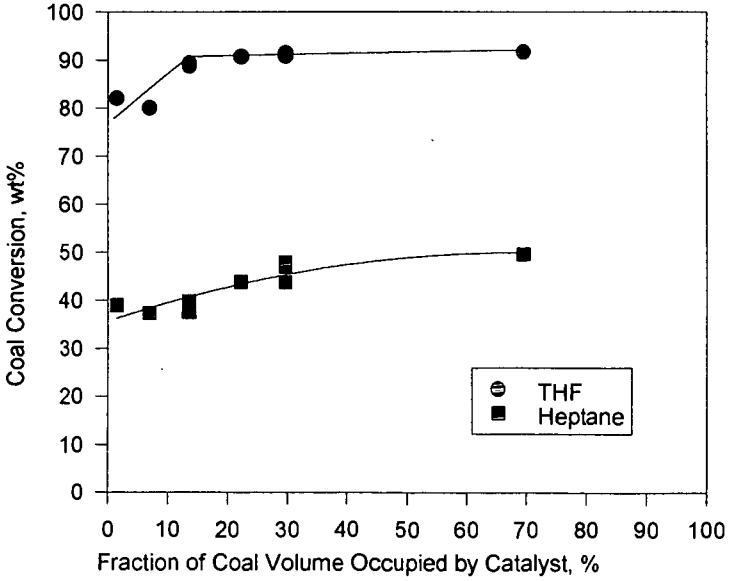

2:1 PANASOL to Coal, 425°C, 1000 ppm Mo, 1000 psig H_2 (cold), and 0.5 h

Preparation of Highly Dispersed NiMo Catalysts Supported on Carbon Black Particles of Hollow Spheres

Kinya Sakanishi, Haru-umi Hasuo, Isao Mochida, and Osamu Okuma[+)]
Institute of Advanced Material Study, Kyushu University,
Kasuga, Fukuoka 816, Japan
[+)] Polymer & Chemical Technology Lab., Kobe Steel,Ltd.,
Kobe, Hyogo 651-22, Japan

Abstract

One of unique carbon blacks, Ketjen Black(KB) which has extremely high surface area and low specific gravity, was selected as a catalyst support to prepare a highly dispersed NiMo catalyst for the hydrogenation of 1-methylnaphthalene(1-MN) using a magnetic-stirred autoclave of 50 ml capacity under the standard conditions of 380℃, 40 min, and 10 MPa H_2 reaction pressure.The catalyst, prepared from Mo dioxyacethylacetonate (MoO_2-AA) and $Ni(OAc)_2$(Ni acetate) in their methanol solution by successive impregnations of Mo(10 wt%) and Ni(2 wt%), provided the highest conversion of 84 % to methyltetralins . Combinations of metal salts soluble in organic solvent, impregnation solvents, and surface properties of carbon black are suggested to be very important for the preparation of highly active catalysts. The nitric aicd treatment introduced a large number of oxygen functional groups to the carbon black to improve the dispersion of water-soluble metal salts. It is also noted that KB-supported NiMo catalysts showed much higher activity for the present hydrogenation than a commercial $NiMo/Al_2O_3$.

Introduction

NiMo and CoMo catalysts supported on alumina extrudates have been extensively applied to the petroleum refineries as hydrotreating catalysts. Alumina is believed one of the best supports because it has large surface area for high dispersion of metals and high mechanical strength for the utilization to the conventional fixed bed flow-reactors. However, such alumina -supported Mo-based catalysts often suffur coking and plugging problems due to the acidity of alumina and the limited activity for the heavy polyaromatic hydrocarbons.[1-3] Hence, recently Ca-modified $NiMo/Al_2O_3$ and fine particle Mo catalysts used in dispered phase as well as the modified aluminas of controlled surface properties have been developed for the suppression of catalyst deactivation due to the coke formation.[4-6]

Titania and carbon supports have attracted much attention for the preparation of anti-coking Mo-based catalysts because of their moderate polarity and metal dispersion ability[7-10]. Carbon supported catalysts can be recovered after the reactions by gravimetric separation due to their low specific gravity and hydrophobic prperties for phase separation[11,12].

In the present study, Ketjen Black(KB), one of unique carbon blacks with extremely high surface area and low specific gravity, was selected as the support for NiMo. Ketjen Black(KB) particles have hollow spheric structure which brings about their extremely high surface area of ca. 1000 m^2/g for high dispersion of active species and low specific gravity for catalyst recovery.[13] Fine sphere without pore may be most suitable for th e catalyst support for the heavy hydrocarbon. Carbon blacks have been reported to exhibit some catalytic activity for hydrocracking reaction due to its positively charged surface and high surface area with functional groups.[14,15]

Such KB-supported NiMo catalysts are one of the most promising catalysts which have the fairly large activity for hydrogenation and liquefaction at the least aount of catalyst with the function for the recovery by gravimetric separation.

Experimental

Some properties of Ketjen Black(KB) ED and JD used in the present study are summarized in Table 1. Ni, Mo-supported KB catalysts (NiMo/KB) were prepared by impregnating,methods using $Ni(NO_3)_2$ or $Ni(OAc)_2$ as Ni salts, and $(NH_4)_6Mo_7O_{24}$, $Mo(CO)_6$ or Mo dioxyacetylacetonate (MoO_2-AA) in water, methanol and their 9:1 mixture, or n-hexane according to the solubility of the salts. The catalyst precursors were dried at 120℃ for 12 h in vacuo and presulfided in 5% H_2S/H_2 flow at 360℃ for 3 h prior to the reactions. KB was pretreated in conc. nitric acid at 80℃ for 1 h followed by filtration, repeated washing with water, and drying at 120℃ in vacuo. The nitric acid-treated KB JD was abbreviated as KB JD-O, which was used for improved dispersion of metal species. A commercially available $NiMo/Al_2O_3$(KF-842) provided by Nippon Ketjen Co., was used for the comparison with the KB-supported NiMo catalysts.

1-Methylnaphthalene(1-MN; 1.0g), decalin(9.0g) and catalyst (5 wt% based on 1-MN) were charged into the autoclave of 50 ml capacity. Standard conditions for the hydrogenation were 380℃-40min and 10MPa H_2 of reaction pressure. The conversion to hydrogenated products of 1- and 5-methyltetralins and their selectivity were determined by GC and GC-MS to estimate the hydrogenation activity of the catalysts.

Results and Discussions

The hydrogenation activities of KB-supported NiMo catalysts are shown in Figure 1 . KB JD which has a larger surface area of 1270 m^2/g exhibited a little higher activity for 1-MN hydrogenation than KB EC(800 m^2/g). The nitric acid-treated KB JD (KB JD-O) provided its supported NiMo catalyst with higher hydrogenation conversion of 60 %, increasing the selectivity to 1-methyltetralin (1-MT). The nitric acid treatment of carbon black introduced oxygen functional groups, improving the dispersion of metal salts on the carbon black support.

Figures 2 shows the effects of the species of Ni and Mo salts using KB JD support on the hydrogenation activity. The Mo species were very influential on the catalytic activity in combination with $Ni(NO_3)_2$ and KB JD support .

The combination of MoO_2- AA with $Ni(NO_3)_2$ in methanol solvent improved the hydrogenation conversion upto 82% ,suggesting that the balanced solubilities of Ni and Mo salts in impregnation solvent may be very important for preparing the highly dispersed NiMo catalyst on KB.

The activities of KB-supported NiMo catalyst are compared with a commercial $NiMo/Al_2O_3$ catalyst(KF-842) in Figure 3. The KB-supported NiMo catalyst of the highest activity, prepared from the successive impregnations of MoO_2-AA and $Ni(OAc)_2$ in methanol supported on KB JD, provided the 1-MN conversions of 84% and 47% respectively by the catalyst amounts of 5 wt%and 1%,reapectively. On the other hand, powdered the commercial $NiMo/Al_2O_3$ (*60mesh* pass) exhibited a lower conversion when 5 wt% of the catalyst was applied . The reaction rates of KB-supported and commercial NiMo catalyst under conditions of 380℃ ,10MPa H_2 reaction pressure by 1wt% catalyst amount are $v = 1.7949 \times 10^{-4}$ and 4.1287×10^{-5}, respectively. The KB catalyst has about 4.4 times more active than that of the commercial catalyst (see Figure 4).

Figures 5 and 6 show the effects of reaction pressure and temperature on 1-MN hydrogenation for NiMo/KB and KF-842. The KB-supported NiMo catalyst exhibited sharp increase of activity by increasing pressure to 7.0MPa H_2 . Further increase of pressure increased moderately. In contrast , KF-842 did very moderate increase upto 10MPa.

The NiMo/KB showed significant activity at 320℃ and increased its activity at higher temperature upto 360℃ . Further higher temperature reduced the activity probable due to equilibrium limitation . KF-842required to show its significant activity .

Conclusion

KB supported NiMo was found very active for the hydrogenation of 1-methylnaphthalene, exceeding very much a commercial NiMo alumina catalyst of similar metal loading level. The activity at lower temperature and pressure should be noted.

Kind and pretreatment of KB and supporting procedure were influential on the catalytic activity . The larger surface tends to give higher activity . The oxidation treatment was effective for the impregnation from the aqueous solution, while the impregnation from the organic solution gave the highest activity to the as-recieved KB with organic soluble salts of MoO_2-AA and $Ni(OAc)_2$.

References

1) Groot,C.K., de Beer,V.H.J., Prins,R., Stolarski,M., Niedzwiedz,W.S., Ind.Eng. Chem.Prod.Res.Dev., 1986, 25, 522-530.
2) Hillerova,E., Vit,Z., Zdrazil,M., Shkuripat,S.A., Bogdanets,E.N., Startsev, A.N.,Appl. Catal., 1991, 67, 231-236.
3) Louwers,S.P.A., Prins,R., J.Catal., 1992, 133, 94-111.
4) Kageyama,Y., Masuyama,T., Proc.Int.Conf.Coal Sci., 1985, p.157-160.
5) Paradhan,V.R., Herrick,D.E., Tierney,J.W., Wender,I., Energy & Fuels,1991, 5, 712
6) Kim,S.I., Woo,S.I., J.Catal., 1992, 133, 124-135.
7) Mochida,I., Oishi,T., Korai,Y., Fujitsu,H., Ind.Eng.Chem. Prod.Res.Dev., 1984, 23, 203.
8) Japanese Patent, Showa57-132547(1982).
9) Duchet,J.C., van Oers,E.M., de Beer,V.H.J., Prins,R., J.Catal., 1983, 80, 386-402
10) Derbyshire, F.J., DeBeer, V.H.J., Abotsi, G.M.K., Scaroni, A.W., Solar, J.M., Skrovanok,D.J., Appl.Catal., 1986, 27, 117.
11) Schmitt,J.L., Castellion,G.A., US Patent 3,997,473(1976)
12) Schmitt,J.L., Castellion,G.A., US Patent 4,032,435(1977)
13) Nelson,J.R., Wissing,W.K., Carbon, 1986, 24, 115-121.
14) Farcasiu,M., Smith,C., Energy & Fuels, 1991, 5, 83.
15) Farcasiu,M., Smith,C., Prepr.ACS Div.Fuel Chem., 1990, 35, 404.

Table 1 Some proparties of Ketjen Blacks

	KB EC	KB EC600JD
Surface area(m /g)	800	1270
Volatile matter(%)	0.5	0.7
pH	9.0	9.0
Particle size (nm)	30	30
Apparent density (g/l)	145	115
Ash (%)	0.1	0.1

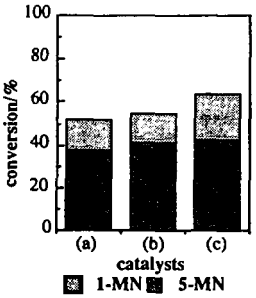

Reaction conditions
Reaction temp.: 380℃
Reaction press.: 10MPa
Heating rate : 10℃/min
catalyst : 5wt% (based on1-MN, simultaneous impregnation from $Ni(NO_3)_2$ and $(NH_4)_6Mo_7O_{24}$)

catalysts support
(a) KB EC
(b)KB JD
(c) KB JD-O

Fig.1 Effect of support species on 1-MN Hydrogenation(HYD).

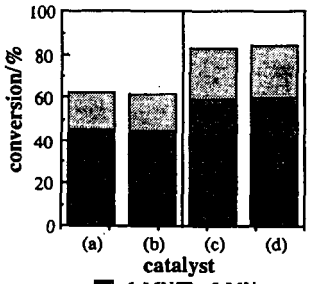

Fig.2 Effect of metal salts combination in organic solution on 1-MN HYD.

metal salts
(a) $Mo(CO)_6$,$Ni(NO_3)_2$
(b) $Mo(CO)_6$,$Ni(OAc)_2$
(c) MoO_2-AA,$Ni(NO_3)_2$
(d) MoO_2-AA,$Ni(OAc)_2$

support : KB JD
successive impregnation in methanol

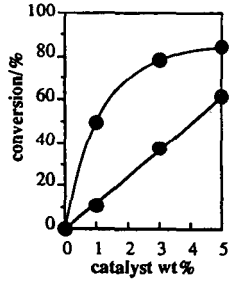

Fig.3 Effect of amount of catalysts on 1-MN HYD.

● KF-842 (60mesh under)
● Ni-Mo/KB JD
(MoO_2-AA,$Ni(OAc)_2$)

(Other conditions are same as Fig. 1)

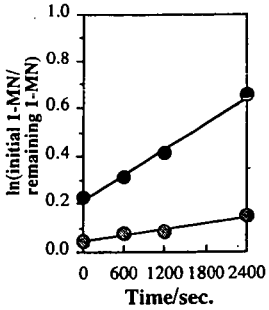

Reaction conditions
Reaction temp.: 380℃
Reaction press.: 10MPa
Heating rate : 10℃/min
catalyst : 1wt%(based on 1-MN)

Ni-Mo/KB JD $\nu = 1.7949 \times 10^{-4}$
KF-842 $\nu = 4.1287 \times 10^{-5}$

● KF-842 (60mesh under)
● Ni-Mo/KB JD
(MoO2-AA,Ni(OAc)2)

Fig. 4 Comparison of commercial NiMoand KB-supported NiMo catalysts in the hydrogenation of 1-MN

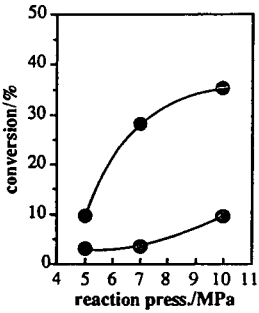

Fig.5 Effect of reaction pressure on 1-MN HYD.

● KF-842 (60mesh under)
● Ni-Mo/KB JD
(MoO2-AA,Ni(OAc)2)
Reaction pressure :5.0~10MPa
Reaction Time : 40min

(Other conditions are same as Fig.4)

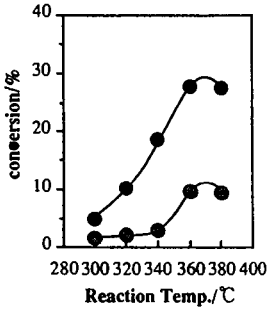

Fig. 6 Effect of reaction temperature on 1-MN HYD.

● KF-842 (60mesh under)
● Ni-Mo/KB JD
(MoO2-AA,Ni(OAc)2)
Reaction temp.: 300~380℃
Reaction time : 40min

(Other conditions are same as Fig.4)

The Activity of Nanoscale Iron Oxide for Model Compound Reactions

G. T. Hager, K. D. Greer, E. N. Givens, F. J. Derbyshire
Center for Applied Energy Research
University of Kentucky
3572 Iron Works Pike
Lexington, KY 40511-8433

Abstract

Iron based catalysts have long been known to enhance the conversion in a direct coal liquefaction process. Attempts to increase the moderate activity of these catalysts have focussed on reducing particle size, enhancing and maintaining dispersion, and modifying the structure by addition of promoters. Sulfated hematites have been reported in the literature to exhibit significant activity for low rank coal liquefaction. The use of promoter metals such as molybdenum and tungsten has been shown to further enhance the catalytic effect. The superacidity of these particles has been suggested as a possible explanation for their high activity. The purpose of this study was to ascertain the effect of various promoter metals, both individually and in combinations on different types of reactions commonly associated with coal liquefaction.

Introduction

Iron based dispersed catalysts have been utilized in direct coal liquefaction since the early 1900's, particularly for the liquefaction of low rank coals. Continuing efforts have been directed at improving the activity of these catalysts without significant increases in cost. These efforts have focussed on reducing the particle size, enhancing and maintaining the dispersion, and modifying the structure by addition of promoters.

Several studies have demonstrated the high activity of sulfated hematite for both coal liquefaction, and coprocessing of coal with a petroleum resid.[1,2,3] The use of molybdenum or tungsten as a promoter metal further improved the activity of these particles.[4,5] Other research has examined nickel, cobalt, tungsten, and molybdenum as promoter metals, both individually and in combination.[6] Molybdenum produced the largest increase in activity for singly-promoted sulfated hematite. The influence of tungsten, when used in combination with molybdenum, was essentially additive while the combination of nickel or cobalt with molybdenum exhibited synergistic effects, resulting in enhanced conversions at low promoter loading.

The role of catalysts in coal liquefaction is obscured by the complexity of the coal itself. In order to more clearly understand the role of these promoter metals in enhancing the activity of sulfated hematite catalysts for coal liquefaction, they have been studied in the reactions of selected model compounds. The activity for cleavage of the sulfur bridges may be studied by the hydrodesulfurization (HDS) of benzothiophene. Similarly, the activity for cleavage of the etheric bond may be inferred from the hydrodeoxygenation (HDO) of diphenyl ether and the activity for nitrogen removal by the hydrodenitrogenation (HDN) of quinoline. Hydrogenation (HYD) activity of the catalyst may be studied by the conversionof naphthalene to tetralin.

Experimental

Ractions were carried out using 25 ml stainless steel microautoclave reactors. The reactors were loaded with 5 g of a 5 wt% solution of reactant in hexadecane. The catalysts were loaded at 5 wt% on a reactant basis and 0.017 g dimethyldisulfide (DMDS) was added in most runs. The reactors were purged and pressurized to 800 psig (cold) with hydrogen. The loaded reactors were placed in a heated fluidized sand bath at 385°C and agitated vertically at 400 cycles/minute to minimized any mass transfer constraints. The reactions were carried out for times of 15 to 60 minutes after which the reactor was quenched in a cool sand bath.

The reaction products were removed from the reactor by washing with tetrahydrofuran. A gas chromatograph (Hewlett Packard 5890 Series 2) using both a 30 m DB-5 and a 30m carbowax column was utilized to analyze the products of the reaction. The catalyst activity was determined by the rate of model compound disappearance.

The spent catalyst was collected and stored with the product to reduce oxidation from exposure to air. The major phases present in the catalyst particles were determined by X-ray diffraction (XRD) and the average particle diameter was estimated from the peak broadening using the Debye-Scherrer relationship.

Catalyst Synthesis and Characterization

The iron based catalysts used in this study were prepared using an aqueous precipitation technique. This method involves the coprecipitation of iron and a promoter metal in the presence of sulfate ions. In this study, urea was used to effect the precipitation of ferric ammonium sulfate (iron alum), following the method of Kotanigawa et al.[1] The promoter metal molybdenum was incorporated by addition of ammonium molybdate to the iron alum solution, as described previously.[6] Ammonium nickel sulfate hydrate and cobalt sulfate hydrate were used to add nickel and cobalt, respectively. The precipitated catalysts were filtered and dried in an air flow oven overnight and then calcined in air at 475 °C for 30 minutes.

The promoted sulfated hematite catalysts were analyzed by a variety of techniques. The results of electron microscopy analysis have shown that the catalysts consist of a loose agglomeration of particles, with acicular shape and average dimensions of ~10x50 nm. Surface areas measured by nitrogen BET adsorption were found to be in the range of 100-200 m^2/g. The addition of up to 10 wt% of molybdenum had little effect on the particle size and no apparent effect on the major phase identified by XRD. The XRD spectra of the as-formed catalysts indicate that the major phase is α-FeOOH, although the crystallinity was poorly developed. After calcination the major phase was clearly identified as α-Fe_2O_3.

Elemental analysis of the sulfated hematites indicated sulfur contents of 2-6 wt%. The results of metals analysis are shown in Table 1. Molybdenum is more easily added to the catalyst resulting in a higher concentration than nickel or cobalt. XPS studies have indicated that the molybdenum is present on the surface of the particles while nickel and cobalt are substituted for iron in the particles.[6]

Results

The results of the naphthalene hydrogenation studies are shown in Figure 1. All runs were conducted with an excess of sulfur present to assure complete sulfidation of the catalyst. The unpromoted sulfated hematite resulted in an increase in conversion of ~20% over the thermal baseline. Promotion by nickel and cobalt appeared to slightly inhibit the activity of these catalysts for the hydrogenation reaction. Molybdenum had a very positive effect, producing an increase in naphthalene hydrogenation of ~50% over the unpromoted sulfated hematite after 60 minutes. This result can be related to the high concentration of molybdenum and its well known hydrogenation properties. The data indicate that the catalysts experience an initial period of low activity before the activity begins to increase, as clearly displayed by the molybdenum promoted catalyst. This induction period may correspond to the conversion of the catalyst from the oxide phase to a sulfide phase. XRD spectra of the catalyst recovered from 15 minute runs indicate that pyrrhotite is the major phase present. The activity of the catalyst prior to conversion to the sulfide may be significantly lower than the activity after conversion. Studies at shorter times should help to elucidate the rate of activation the catalysts.

The catalysts followed a similar trend for the HDO of diphenyl ether, as shown in Figure 2. Unpromoted sulfated hematite caused a significant increase over the thermal runs giving a conversion of 40% at 60 minutes. Nickel and cobalt promoters were found to have little additional effect, but molybdenum produced a significant increase to 57% after 60 minutes. The major reactions appears to involve cleavage of one of the carbon oxygen bonds resulting in the formation of equal amounts of benzene and phenol with

some further hydrogenation to cyclohexane and cyclohexanol, respectively. Only the molybdenum promoted catalyst resulted in a slight (<5%) amount of oxygen removal.

Both oxide and sulfide forms of Co/Mo supported on alumina are known to exhibit high activity for HDN reactions [7], which may help to explain the rapid reaction rates seen in the studies of quinoline HDN, shown in Figure 3. As observed in the previous reactions, the nickel and cobalt promoters had little effect on the activity of the sulfated hematite, and all three catalysts resulted in a significant increase in conversion over the thermal baseline. Again, the molybdenum promoted catalyst had the most significant effect on rate of quinoline conversion. The main product in all the reactions was 1,2,3,4 tetrahydroquinoline and very little HDN was observed for any of the catalyst.

It has been suggested that the superacidity associated with the sulfate groups chemisorbed on the surface of the hematite particles may explain some of the catalyst function.[2] This type of acidity should result in significant cracking of the hexadecane solvent used in this study. Since no significant increase in cracking was observed in these experiments, it would appear that the superacid sites are no longer present under reaction conditions.

Conclusions

Sulfated hematite catalysts appear to exhibit moderate activity for hydrogenation reactions. The use of nickel and cobalt as promoter metals had only slight effect on the activity of the sulfated hematite. Molybdenum promoted sulfated hematite showed significantly higher activity than the unpromoted catalyst. This agrees well with the results from coal liquefaction experiments. From these investigations it would appear that hydrogenation and ether cleavage are relevent catalyst functions in the liquefaction of a low rank coal.

Acknowledgements

The authors would like to gratefully acknowledge support for this project received from the United States Department of Energy under contracts DE-AC22-91PC91040.

References

1. Kotanigawa, T., Yokoyama, S., Yamamoto, M. & Maekawa, Y. *Fuel* **68**, 618-621 (1989).
2. Pradhan, V.R., Tierney, J.W., Wender, I. & Huffman, G.P. *Energy & Fuels* **5**, 497-507 (1991).
3. Pradhan, V., Tierney, J.W. & Wender, I. *ACS Preprint - Fuel* **36**, 597-604 (1991).
4. Pradhan, V.R., Herrick, D.E., Tierney, J.W. & Wender, I. *Energy & Fuels* **5**, 712-720 (1991).
5. Pradhan, V.R., Hu, J., Tierney, J.W. & Wender, I. *Energy & Fuels* **7**, 446-454 (1993).
6. Hager, G.T., Givens, E.N. & Derbyshire, F.J. *ACS-Division of Fuel Chemistry Preprints* **38**, 1087-1092 (1993).
7. Gates, B.C., Katzer, J.R., &Schuit, G.C.A. Chemistry of Catalytic Processes, McGraw-Hill, New York 464 pp (1979).

Table 1. Elemental Analysis of Promoted Catalysts.

Promoter Metal	Promoter Concentration (wt%)
Nickel	1.8%
Cobalt	2.0%
Molybdenum	8.0%

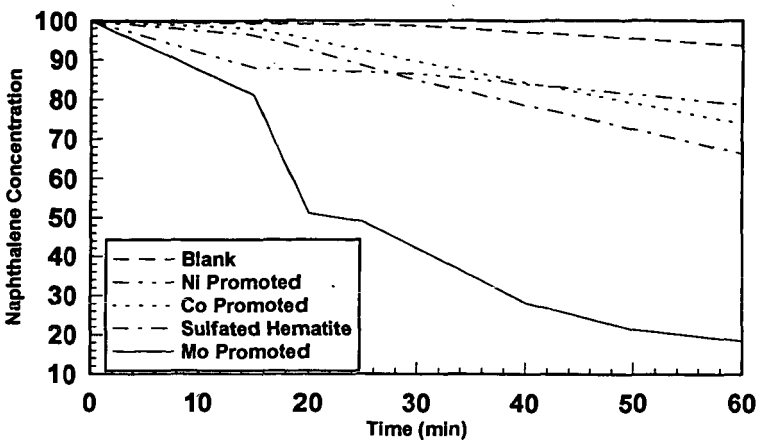

Figure 1. Hydrogenation of Naphthalene

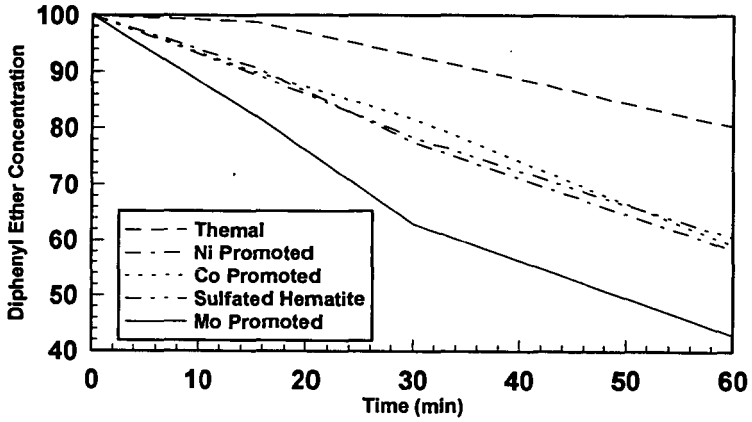

Figure2. HDO of Diphenyl Ether

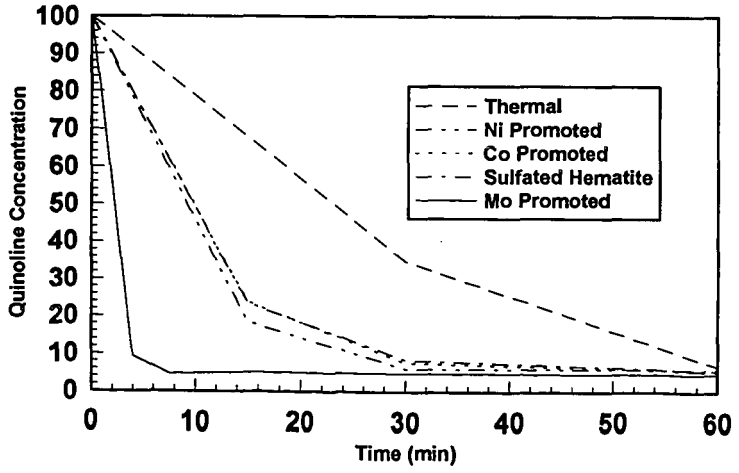

Figure 3. HDN of Quinoline